IOWA STATE UNIVERSITY
Digital Repository

1966

Stimulated compton scattering of electrons by a laser beam

Roland Rufus Roskos
Iowa State University

Recommended Citation

www.manaraa.com

STIMULATED COMPTON SCATTERING

OF ELECTRONS BY A LASER BEAM

by

Roland Rufus Roskos

A Dissertation Submitted to the

Graduate Faculty in Partial Fulfillment of

The Requirements for the Degree of

DOCTOR OF PHILOSOPHY

Major Subject: Physical Chemistry

Approved:

Signature was redacted for privacy.

In Charge of Major Work

Signature was redacted for privacy.

Head of Major Department

Signature was redacted for privacy.

Dean of Graduate College

Iowa State University
Of Science and Technology
Ames, Iowa

1966

TABLE OF CONTENTS

INTRODUCTION

In 1933, P. L. Kapitza and P. A. M. Dirac (1) of England predicted

the existence of stimulated Compton scattering, i.e. the reflection of

electrons by standing light waves. According to the wave picture, the

reflection of a monochromatic light perpendicularily from a mirror causes

the incident and reflected waves to interact and form standing light

waves. The two wave trains reinforce and cancel each other to form sta-

tionary nodes (positions of zero light intensity) alternating with regions

of high intensity. Planes of periodic photon density can presumably re-

flect an electron beam, provided Bragg's law is satisfied,

$$n\lambda_{el} = 2(\lambda_{ph}/2) \sin \theta$$

where $\lambda_{ph}/2$ is the repeat distance, λ_{ph} is the photon wavelength, λ_{el}

is the electron wavelength, θ is the Bragg angle for maximum scattering

and n is either zero or one.

It was, however, the corpuscular picture which led Kapitza and

Dirac to designate the phenomena as stimulated Compton scattering.

A standing light wave can be viewed as a superposition of two running

waves equal in amplitude and frequency and traveling in opposite direct-

ions. An electron suitably aimed to intersect the Bragg planes can

absorb a photon from an incoming wave. Stimulated emission can then

be induced by an incoming or outgoing wave at 0° or 180° respectively.

The photon change of momentum is either zero or $2h/\lambda_{ph}$. The trajec-

tory of the recoiling electron satisfies Bragg's law as a consequence

of energy and momentum conservation. Photon emissions at 0° and with

zero momentum exchange correspond to zero order Bragg reflections, and

photon emissions at 180° and with a momentum exchange of $2h/\lambda_{ph}$ corres-

pond to first order Bragg reflections.

A comparison of the stimulated Compton effect with ordinary Comp-

ton scattering (2-4) might be fruitful. In inelastic or ordinary Comp-

ton scattering, the collision of a photon and an electron results in a

virtual state from which the photon is later spontaneously emitted in

some arbitrary direction. The momentum exchange from photon to electron

must be less than $2h/\lambda_{ph}$, and depends on the direction of emission. In

elastic stimulated Compton scattering, the photon emission from a vir-

tual state is restricted in direction and the momentum exchange is

quantized to zero or $2h/\lambda_{ph}$. Ordinary Compton scattering will be the

only observed interaction between matter and radiation when electrons

intersect an intense light beam propagating in a single direction. If

the electrons intersect an intense light beam propagating in opposite

directions, i.e. standing light waves, both types of interactions might

be observed. With high intensity light, stimulated Compton scattering can

predominate because scattering probabilities are proportional to the

square of photon intensity. Probabilities for ordinary Compton scat-

tering, however, are proportional to the first power of the photon in-

tensity.

At the time Kapitza and Dirac proposed their theory, available

light sources restricted scattering probabilities to about 10^{-14}, and

stimulated Compton scattering remained outside the realm of experimental

reality. Discovery of the laser as a monochromatic, coherent, and intense

light source, however, creates a new interest. The standing waves set up in a laser cavity seem ideal for scattering electrons. Experimental observation of stimulated Compton scattering should now be possible.

The formulations of Kapitza and Dirac are not directly applicable to the new experimental conditions. Doctor Bartell has recently treated stimulated Compton scattering in terms of an interaction of an electron plane wave with a perturbing potential corresponding to a standing light wave, and the Born approximation to obtain a stationary state solution to the Schrodinger equation. Probabilities of electron deflection were derived for various possible laboratory conditions with emphasis placed on electron beam orientation, coherence properties of the laser, as well as divergence specifications of a system.

THEORY

Formulation of Kapitza and Dirac

Kapitza and Dirac (1) derived an expression for the probability of stimulated Compton scattering by combining ordinary Compton scattering theory with the ratio of Einstein coefficients for stimulated emission and spontaneous emission. The intensity of a scattered light beam by a single electron according to Thomson's formula is

$$I_\omega = \frac{e^4}{m^2 c^4} I_o \qquad (1)$$

where I_o is the energy of an incident beam of light per unit area per unit time, I_ω is the energy of light scattered in the backward direction per unit solid angle per unit time, e is the electronic charge, m is the mass of the electron, and c is the speed of light. For non-polarized light, one can pass from a non-stimulated effect to the stimulated effect by multiplying the right side of Equation 1 by

$$\frac{c^2}{2h\nu^3} I'_{\omega\nu} \qquad (2)$$

where $I'_{\omega\nu}$ is energy of the stimulating beam of light per unit area per unit solid angle per unit time per unit frequency range, h is Planck's constant, and ν is the frequency of light. The stimulating beam is spread through a small solid angle $d\omega$; consequently, the stimulated emitted beam will also be spread through the same solid angle and the total energy per unit time will be

$$I_\omega \, d\omega = \frac{e^4}{m^2 c^4} I_o \cdot \frac{c^2}{2h\nu^3} I'_{\omega\nu} \, d\omega$$

$$= \frac{e^4}{2m^2 c^2 h\nu^3} I_o I'_\nu \tag{3}$$

where $I'_\nu = I'_{\omega\nu} \, d\omega$ is the energy of the stimulating beam per unit area
per unit time per unit frequency range. The probability of a stimu-
lated event per unit time for one electron can be obtained by dividing
both sides of Equation 3 by $h\nu$, the energy of one quantum. If the length
of standing waves through which the electron must pass is ℓ and the ve-
locity of the electron is v, then the time the electron spends in the
perturbing field is given by ℓ/v. The probability then takes the form

$$P = \frac{e^4 \ell}{2m^2 c^2 h^2 \nu^4 v} I_o I'_\nu \, . \tag{4}$$

The beam of I_o, however, consists of a narrow spectral line of radiation
of finite breadth and can be expressed as

$$I_o = \int I_\nu \, d\nu$$

where I_ν is the energy per unit area per unit time per unit frequency
range. Each element of frequency range $d\nu$ will contribute to the term
$I_o I'_\nu$ and amount $I_\nu I'_\nu \, d\nu$. Consequently,

$$P = \frac{e^4 \ell}{2m^2 c^2 h^2 \nu^4 v} \int I_\nu I'_\nu \, d\nu \, . \tag{5}$$

The preceding treatment deals with unpolarized light where the
x component cannot stimulate emission in the virtually absorbed y

component and vice-versa. Since in polarized radiation all rays have

the same direction, the factor of two drops out of Equation 5,

$$P = \frac{e^4 \ell}{m^2 c^2 h^2 \nu^4 v} \frac{I_o I_o'}{\Delta \nu^2} \tag{6}$$

where $\Delta \nu$ is defined by

$$\int I_\nu I_\nu' \, d\nu = \frac{I_o I_o'}{\Delta \nu} \, . \tag{7}$$

Extended Theoretical Treatment

The probability that an electron will undergo stimulated Compton

scattering by a standing light wave will be derived for several well

defined conditions. It will be shown, among other things, that the ori-

ginal formula of Kapitza and Dirac requires modification before it can

be compared with experimental studies with lasers.

We shall treat stimulated Compton scattering in terms of the inter-

action of an electron plane wave with the periodic perturbing potential

corresponding to a standing light wave. For a small perturbing field the

solution to the Schrodinger equation is given by the Born approximation[5]

$$\mathcal{J}(\phi) = \mathcal{J}_o (2\pi m/h^2 R)^2 \left| \int e^{i\vec{s}\cdot\vec{r}} V(\vec{r}) \, d\tau \right|^2 \tag{8}$$

where $\mathcal{J}_o$ is the incident electron intensity, m is the electron mass,

R the distance between the scatterer and the point of detection, $\vec{r}$ the

position in the scattering medium, and $V(\vec{r})$ the potential energy of an

electron in the scattering medium. If $\vec{n}_o$ and $\vec{n}$ are unit vectors in the

direction of the incident and scattered electron beams, $\vec{s}$ is a vector of

direction $(\vec{n}_o - \vec{n})$ and magnitude $(4\pi/\lambda_e) \sin (\theta/2)$. Equation 8 expresses the scattered electron intensity $\mathcal{J}(\phi)$ as a function of the scattering angle ϕ.

For the purposes of the problem, $V(r)$ is given adequately by the potential energy of an electron in a classical radiation field, or

$$V(\vec{r}) = -(e/mc) \, \vec{A} \cdot \vec{p} + (e^2/2mc^2) \, |\vec{A}|^2 \qquad (9)$$

where $\vec{A}$ is the vector potential. In conventional one photon processes involving bound electrons (absorption, emission, etc.) the $\vec{A} \cdot \vec{p}$ term is overwhelmingly the leading term. Two photon processes with bound electrons (two photon absorption, one photon absorption to virtual state followed by emission, etc.) result in first order from the $|\vec{A}|^2$ term and second order from the $\vec{A} \cdot \vec{p}$ term. In the case of a free electron, however, to second order the only contributor is the $|\vec{A}|^2$ term.

In the following sections we shall apply the above treatment to several situations, starting with the simplest case, the scattering of electrons by a perfectly coherent light wave.

Standing wave of monochromatic light

Let us assume that the light waves are plane waves moving along the z-axis with no spread in wavelength. The vector potentials of the components in the standing wave may be written as

$$A(z,t) = A_o \cos (kz + \omega t) \qquad (10a)$$

and

$$A'(z,t) = A_o' \cos (kz - \omega t) \qquad (10b)$$

in which $k = 2\pi/\lambda_p$ and $\omega = 2\pi\nu$. Here and later, symbols for wave trains running upward are primed whereas symbols for wave trains running downward

are left unprimed. We assume that both wave trains are plane polarized in the same direction, but the particular direction is immaterial in the problem. The expression for $|A|^2$ to be inserted into Equation 9 is

$$(A + A')^2 = 2A_o A_o' \cos^2 kz + (\tfrac{1}{2})(A_o - A_o')^2 + A_o A_o' \cos 2\omega t \qquad (11)$$
$$+ (\tfrac{1}{2}) A_o^2 \cos(2kz + 2\omega t) + (\tfrac{1}{2}) A_o'^2 \cos(2kz - 2\omega t).$$

Of the terms in Equation 11 the latter three are time dependent and, for bound electrons, could contribute to two photon absorption or emission. Since such transitions are not allowed for free electrons, the terms are of no concern in the present problem. The second term corresponds to a featureless dielectric which may refract an electron but which cannot give rise to an interference pattern. The first term corresponds to a stationary diffraction grating with a cosine squared density of "scattering matter" and a repeat distance of $\lambda_p/2$. It is the only term of relevance in this study.

The relationship between the vector potential and intensity of a component running wave is

$$I_o = \pi v^2 A_o^2 / 2c \qquad (12)$$

where I_o is the energy per unit area per unit time.

All quantities required for calculating $\mathscr{J}(\phi)$ by Equation 8 are now at hand. For $V(\vec{r})$, the perturbing potential inside the standing wave may be taken as

$$V(\vec{r}) = (e^2/m^2 c^2) A_o A_o' \cos^2 kz$$

$$= V_o \cos^2 kz. \qquad (13)$$

The scalar product $\vec{s} \cdot \vec{r}$ in Equation 8 may be represented by

$$\vec{s} \cdot \vec{r} = s_x x + s_y y + s_z z$$

$$= sx \sin\beta \cos\gamma + sy \sin\beta \sin\gamma + sz \cos\beta \tag{14}$$

where β and γ are the spherical coordinate angles representing the orientation of $\vec{s}$. For representative conditions β and γ are so small that we may replace s_x, s_y and s_z by βs, $\beta\gamma s$, and s, respectively.

In the experimental arrangement of Figure 1 let us assume the electron beam has a breadth of Y in the y direction (perpendicular to the plane of the figure) and Z in the z direction with $Z \gg \lambda_p$. The integral of Equation 8 becomes, then,

$$\int e^{i\vec{s} \cdot \vec{r}} V(\vec{r}) \, dT = V_o f_x f_y f_z \tag{15}$$

where

$$f_x = \int_{-\ell/2}^{\ell/2} \exp(is_x x) \, dx = (2/\beta s)\sin(\beta s\ell/2) \tag{16a}$$

$$f_y = \int_{-Y/2}^{Y/2} \exp(is_y y) \, dy = (2/s_y) \sin(s_y Y/2) \tag{16b}$$

$$f_z = \int_{-Z/2}^{Z/2} \exp(is_z z) \cos^2 kz \, dz$$

$$= f_+ + f_o + f_- \tag{16c}$$

in which

$$f_o = (1/s) \sin(sZ/2)$$

and

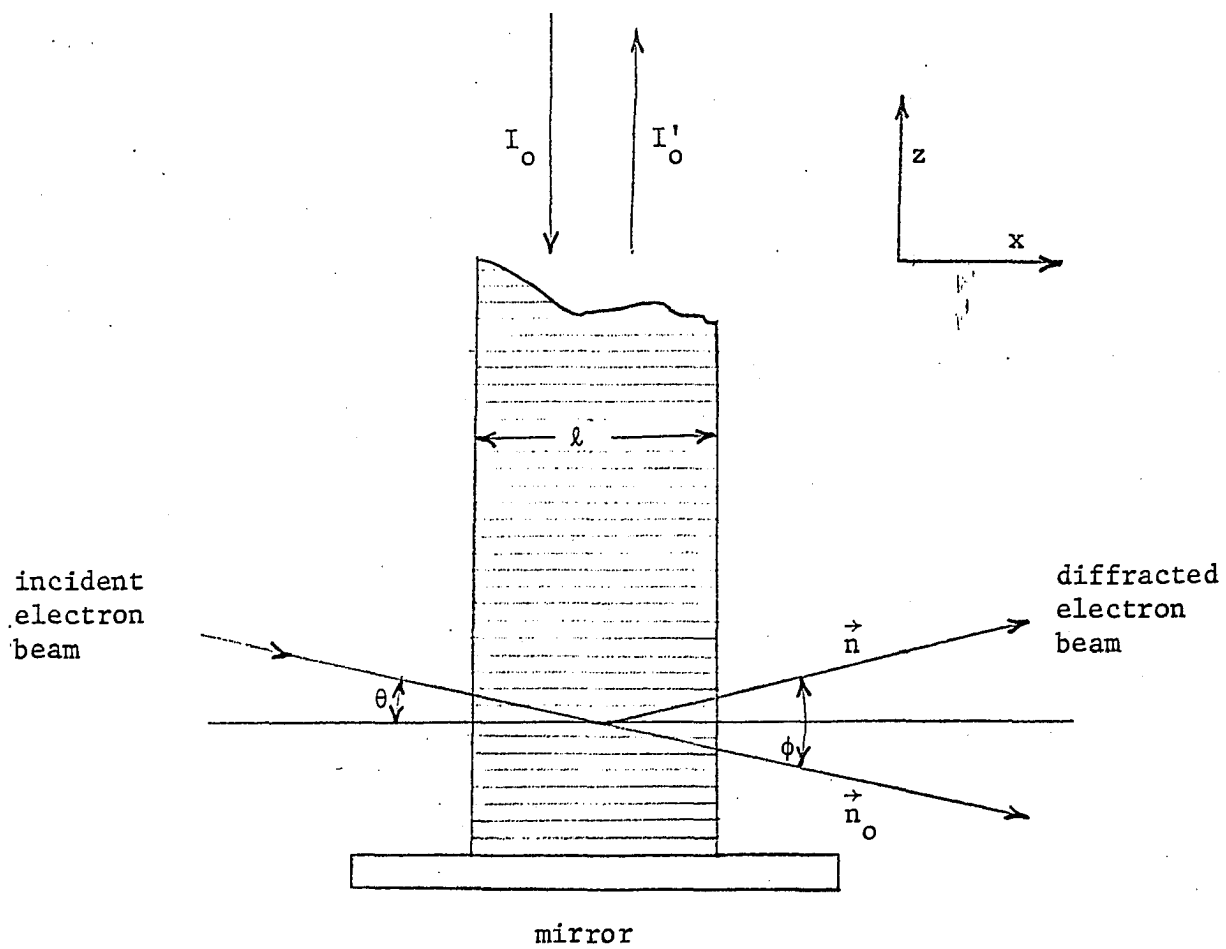$$f_\pm = [1/2(s \mp 2k)] \sin[(s \mp 2k) \, Z/2] \, .$$

Figure 1. Diffraction of electron beam by standing light wave

The factor f_z expresses the requirement that the z axis Laue condition be satisfied. Its components f_o, f_+, and f_- have appreciable values only at scattering angles with $s = 0$ and $s = \pm 2k$, the zeroth order and first order reflections from the photon lattice. The cosine squared form of the density of the scatterer rules out higher order reflections according to Equation 16c. This may be interpreted in terms of the maximum momentum exchange, $2h/\lambda_p$, which a scattered photon can impart. Such an exchange corresponds to a first order reflection.

The factors f_x and f_y increase the severity of the restriction to the full Bragg condition, if ℓ and Y are not too small, by requiring that the reflection be specular. According to Equation 16a, if $\lambda_e \ell/\lambda_p^2 << 1/8$, the factor f_x is no longer very restrictive and the scattering is said to be in the "Raman-Nath" region. Under these not uncommon conditions the orientation of the incident electron beam with respect to the Bragg planes is not critical but the angular variable s is still limited to 0 or $\pm 2k$.

The intensity of scattered electrons is then

$$I(\phi_y, \phi_z) = I_o (2\pi m/h^2 R)^2 \, V_o^2 \, |f_x f_y f_z|^2 \qquad (17)$$

where ϕ_y and ϕ_z are the angles of scattering in the horizontal and vertical directions. At the small scattering angles encountered ϕ_y and ϕ_z may be taken as

$$(\phi/s) = (\phi_y/s_y) = (\phi_z/s_z) \simeq \lambda_e/2\pi \qquad (18)$$

by virtue of the definition of s. For experimental reasons the integrated intensity of the Bragg reflection is of more practical interest than the angular profile of Equation 17. The integrated intensity for a first

order reflection

$$N = \iint \psi_{\pm}(\phi_y, \phi_z) \, R^2 \, d\phi_y \, d\phi_z$$

$$= \left(\frac{N_o}{YZ}\right)\left(\frac{2\pi m}{h^2} \cdot V_o \cdot \frac{\lambda_e}{2\pi}\right)^2 \int_{-\infty}^{\infty} |f_y|^2 \, ds_y \int_{-\infty}^{\infty} |f_x f_{\pm}| \, ds_z \qquad (19)$$

yields the probability N/N_o that an electron in the incident beam will be reflected. Since f_x is virtually constant over the range where $f_{\pm}$ is appreciable, it is easily seen that Equation 19 reduces to

$$N/N_o = (\pi \ell m V_o \lambda_e / 2h)^2 \, g(\beta) \qquad (20)$$

where

$$g(\beta) = [\sin^2 (2\pi\beta\ell/\lambda_p)] \, / \, (2\pi\beta\ell/\lambda_p)^2 \, .$$

The angle $\beta = \theta - \theta_B$ is the deviation between the actual angle θ of entry of the electron beam and the correct Bragg angle θ_B. Consequently, the function $g(\beta)$, which is unity at perfect alignment, expresses the allowable latitude in setting the angle of incidence in a stimulated Compton experiment with an ideal standing wave. Note that even if β is allowed to vary, the total angle of scattering continues to be governed by

$$\lambda_e = 2(\lambda_p/2) \sin (\phi/2) \, .$$

Inserting the deBroglie relation $\lambda_e = h/mv$ and Equations 12 and 13 into Equation 20, we find that the probability $P(\beta)$ of reflection of electrons is

$$P_o(\beta) = N/N_o$$

$$= \left(\frac{\ell e^4}{m^2 c^2 h^2 \nu^4 v}\right) \cdot \left(\frac{\ell}{v}\right) \cdot I_o I_o' \, g(\beta)$$

$$P_o(\beta) = P_\mu \, g(\beta) \tag{21}$$

where P_μ represents the maximum probability of reflection that can be obtained with the light intensities I_o and I_o'. This expression differs from the Kapitza-Dirac relation for $\beta = 0$

$$N/N_o = \left(\frac{\ell e^4}{2m^2 c^2 h^2 \nu^2 \nu'^4} \right) \cdot \frac{I_o I_o'}{\Delta \nu} \, . \tag{22}$$

In Equation 22 the intensities

$$I_o = \int I(\nu) \, d\nu$$

are integrated intensities and $\Delta \nu$ is defined by

$$I_o I_o' / \Delta \nu = \int I(\nu) I'(\nu) \, d\nu$$

in which $I(\nu)$ and $I'(\nu)$ are energies of the component light waves per unit area per unit time per unit frequency range. Equation 22 lacks the ℓ^2/ν^2 dependency of Equation 21 and formally blows up as the frequency spread goes to zero. A closer comparison may be made if it is recognized that there is an effective lower limit of $\Delta \nu$ imposed by the uncertainty principle

$$\Delta \nu_t \cdot \Delta t \geq 1$$

where Δt is the length of time, ℓ/v, that an electron experiences the light wave, or

$$\Delta \nu_t \geq v/\ell \, . \tag{23}$$

For 1-kV electrons passing through a light beam one centimeter wide, v/ℓ is 2×10^9 reciprocal seconds. This corresponds, in the ruby laser,

to $\Delta\lambda_t \simeq 0.03$ Å. If the derivation leading to Equation 22 had been based on plane polarized rather than unpolarized radiation, the factor of two in the denominator would have been absent.

Distribution of frequency and direction of propagation

When the frequency spread $\Delta\nu$ is small compared with ν/ℓ and when the angular divergence of the light waves is small compared with λ_p/ℓ, Equation 21 suffices. Since these conditions are usually not satisfied, it is helpful to derive expressions for the effects of frequency spread and angular divergence of the light.

Let us suppose that an electron encounters two superposed light waves. One, with frequency ν, is moving downward in the xz plane at an angle of η with respect to the z axis. The other is moving up at an angle η', in the same plane, with a frequency ν' slightly different from ν. We may still use the approach of the preceding section if we construct a moving coordinate system in which, by Doppler shifts, the two frequencies are identical and in which, by compensation from lateral motion, the angle between the rays is 180°. In the moving frame of reference the two light waves form a standing wave, the Bragg planes of which can reflect electrons according to Equation 21. If the electron trajectories in the moving frame which satisfy the Bragg relation are transformed back into the laboratory frame, the trajectories can be interpreted in terms of reflections from inclined Bragg planes parallel to the dashed plane in Figure 2. If $(\eta' - \eta)$ and $(\nu' - \nu)$ are small, the angle of inclination ξ is given by

$$\xi = [(\nu' - \nu)c/2\nu\nu] + (\eta' - \eta)/2$$
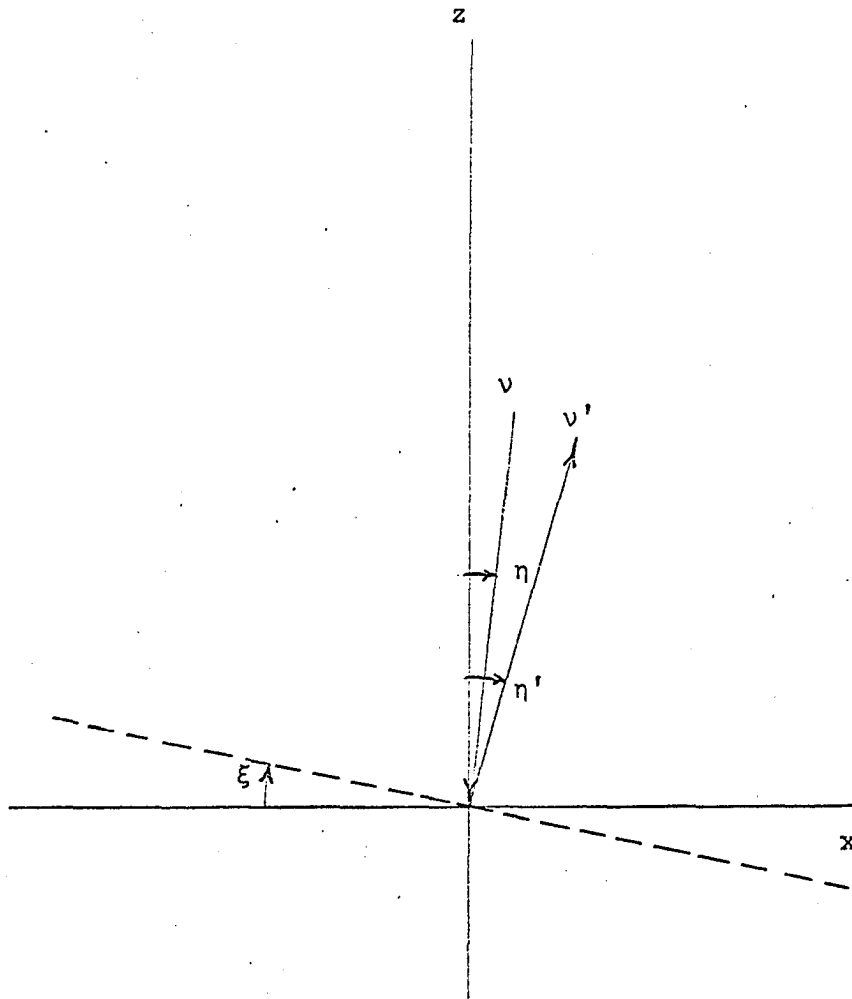
$$= \xi_\nu + \xi_\eta \tag{24}$$

Figure 2. Orientation of effective Bragg planes (parallel to dashed line) when angles and frequencies are different in the absorbed and stimulating light waves

in which the Doppler correction and mean tilt of light rays are evident.

Case with $\Delta\eta = 0$, $\Delta\nu \neq 0$ Let us first consider the case in which
the distribution of ξ values, according to Equation 24, is derived prin-
cipally from the distribution in light frequencies and not from a spread
in ray angles η. This is not the representative case for the output of
a ruby laser but it turns out to be the case corresponding to the treat-
ment of Kapitza and Dirac.

In Equation 24 we express the reflection probability $P_o(\beta)$ as a func-
tion of the Bragg misalignment angle $\beta = \theta - \theta_B$. To extend the treatment
let us continue to reckon β from the effective Bragg planes but let us
refer our results to the laboratory angle β_o, the value of $\theta - \theta_B$ for
hypothetical horizontal Bragg planes. Thus, if the two frequencies ν and
ν' are different, it is apparent from Equation 24 that

$$\beta_o = \beta + \xi_\nu$$

$$= \beta + (\nu' - \nu) \, c/2\nu\nu \qquad\qquad (25)$$

and hence, that the distribution of N/N_o with angle of entry is

$$P_\mu \, g(\beta) = P_\mu \, g(\beta_o - \xi_\nu)$$

$$= P(\beta_o) \; . \qquad\qquad (26)$$

This result is readily extended to the case in which waves of two fre-
quencies ν_1 and ν_2 descend and are each reflected vertically by a mirror,
giving

$$P_\nu(\beta_o) = P_\mu \left\{ \frac{(I_1 I_1' + I_2 I_2') \, g(\beta_o) + I_1 I_2' \, g(\beta_o - \xi_{12}) + I_2 I_1' \, g(\beta_o + \xi_{12})}{I_1 I_1' + I_1 I_2' + I_2 I_1' + I_2 I_2'} \right\}$$

$$(27)$$

where the I_i are intensities of the ith waves and

$$\xi_{12} = (\nu_2 - \nu_1) \, c/2\nu\nu.$$

This result, in turn, may be extended to the case of a continuous distribution of frequencies reflected by a mirror, for which

$$P_\nu(\beta_0) = P_\mu \frac{\iint I(\nu) \, I'(\nu') \, g(\beta_0 - \xi_\nu) \, d\nu \, d\nu'}{\iint I(\nu) \, I'(\nu') \, d\nu \, d\nu'} . \qquad (28)$$

The denominator of Equation 28 can be written as

$$\int I(\nu) \, d\nu \int I'(\nu') \, d\nu' = I_0 I_0' , \qquad (29)$$

the product of total incoming and outgoing intensities.

Equation 28 is the general result for vertically running waves involving a frequency distribution. In the event that the frequency spread is much wider than the limit $\Delta\nu_t$ of Equation 23, the distribution $P_\mu(\beta_0)$ is much wider (and lower) than the $P(\beta)$ of Equation 21. Accordingly, we may treat the function $g(\beta) = g(\beta_0, \nu, \nu')$ as a Dirac delta function. From Equation 25 we see that a frequency ν' will give constructive electron interference when paired with frequency ν at the angle β_0 if the requirement

$$\nu' = \nu + 2\nu\nu\beta_0/c$$

is met. Therefore, we may set

$$g(\beta_0, \nu, \nu') = K \, \delta(\nu' - \nu_0') \qquad (30a)$$

where

$$\nu_0' = \nu + 2\nu\nu\beta_0/c$$

and where the proportionality constant K is determined from the normalization relation

$$1 = \int \delta(\nu' - \nu_0') \, d\nu'$$

$$= K^{-1} \int g(\beta_0 - [\nu' - \nu]c/2\nu\nu) \, d\nu'$$

$$= K^{-1} \int_{-\infty}^{\infty} \left(\frac{\sin \, [\pi\ell(\nu' - \nu_0')/v]}{[\pi\ell(\nu' - \nu_0')/v]} \right)^2 d\nu'$$

$$= v/\ell K$$

or

$$g(\beta_0, \nu, \nu') = (v/\ell) \, \delta(\nu' - \nu_0') \, . \tag{30b}$$

We may now express Equation 28 as

$$P_\nu(\beta_0) = (P_\mu/I_0 I_0') \iint I(\nu) I'(\nu') \, (v/\ell) \, \delta(\nu' - \nu_0') \, d\nu \, d\nu'$$

$$= (v P_\mu/\ell I_0 I_0') \int I(\nu) I'(\nu_0') \, d\nu \, , \tag{31a}$$

or, inserting the value of P_μ from Equation 21,

$$P_\nu(\beta_0) = \frac{\ell e^4}{m^2 c^2 h^2 \nu^4 v} \int I(\nu) I'(\nu + 2\nu\nu\beta_0/c) \, d\nu \, . \tag{31b}$$

At the mean Bragg angle of $\beta_0 = 0$, the reflection probability is at a maximum, and for this special case Equation 31 becomes

$$P_\nu(\beta_0 = 0) = (\ell e^4/m^2 c^2 h^2 \nu^4 v) \int I(\nu) I'(\nu) \, d\nu \, . \tag{32}$$

This is exactly the result derived by Kapitza and Dirac if allowance is made for the fact that Equation 32 pertains to polarized radiation. The polarized case is more appropriate in practice since lasers generate

polarized light and since it is unthinkable, at present, to study the phenomenon without lasers.

It is useful to note that the area

$$\int_{-\infty}^{\infty} P_{\nu}(\beta_o) \, d\beta_o = (\lambda_p/2\ell) \, P_{\mu} \qquad (33)$$

is independent of the frequency spread as long as $\Delta\nu \ll \nu$. Therefore, provided the standing wave is perfectly unidirectional and provided $\Delta\nu \gg \Delta\nu_t$, the effect of doubling $\Delta\nu$ is to double the range of β_o over which reflections may be observed but at the cost of halving the maximum value of N/N_o.

Case with $\Delta\nu = 0$ and $\Delta n \neq 0$ For giant pulse lasers and representative electron velocities the values of $\Delta\nu_t$ and $\Delta\nu$ may be roughly comparable. Therefore, the correct order of magnitude may be calculated from either Equation 21 or Equation 31 in the case of standing waves exhibiting no divergence. On the other hand, the principal assumption of the preceding section is not valid for many or most lasers of high power. If $\Delta\lambda$ for a ruby laser is taken as 0.03 Å, for example, the corresponding range in angle of incidence

$$\Delta\xi = c\Delta\nu/\nu v$$

is only about 3×10^{-5} radians for 1-kV electrons. This is much smaller than the characteristic divergence of several milliradians in laser output. Therefore, it is clear that neither Equation 21 nor the Kapitza-Dirac Equation 31 are likely to be suitable as they stand for interpreting experimental studies with typical lasers. In practical cases, then, the

term ξ_η in Equation 24 arising from the angular divergence of the light waves will often be dominant. The relative tilts of incoming and outgoing waves about the axis of the electron beam (i.e. the tilt components in the yz plane) are of little consequence but the tilt angles which alter the electron's angle of incidence to the effective Bragg planes are important.

Let us now neglect $\Delta\nu$ and take the laboratory angle β_0 to be

$$\beta_0 = \beta + \xi_\eta$$

$$= \beta + (\eta' - \eta)/2 \tag{34}$$

where η and η' refer to projections in the xz plane. If we assume that the waves encountering the mirror may be regarded as a distribution of independent plane waves with different directions we may write equations exactly analogous to Equation 25 - 32. The general result for electron reflection probability close to the mirror is

$$P_\eta(\beta_0) = (P_\mu/I_0 I_0') \iint I(\eta) I'(\eta') \, g(\beta_0 - \xi_\eta) \, d\eta \, d\eta' \tag{35}$$

where

$$I_0 I_0' = \int I(\eta) \, d\eta \int I'(\eta') \, d\eta' .$$

If the spread in η is large compared with the breadth of $g(\beta)$, Equation 35 reduces to

$$P_\eta(\beta_0) = (\lambda_p P_\mu/\ell I_0 I_0') \int I(\eta) I'(\eta + 2\beta_0) \, d\eta \tag{36}$$

or, at the mean Bragg angle of incidence with $\beta_0 = 0$

$$P_\eta(\beta_0 = 0) = (\lambda_p P_\mu/\ell I_0 I_0') \int I(\eta) I'(\eta) \, d\eta. \tag{37}$$

If, for sake of argument, we assume that $I(\eta)$ is of the form

$$I(\eta) = I_o/2\eta_o \, , \qquad |\eta| \leq \eta_o$$

$$= 0 \qquad , \qquad |\eta| > \eta_o$$

the maximum probability $(\beta_o = 0)$ becomes

$$P_\eta(\beta_o = 0) = P_\mu(\lambda_p/\ell)\,(1/2\eta_o)$$

$$= (\ell e^4/m^2 c^2 h^2 \nu^4 v)\,(\lambda_p/2v\eta_o)\,I_o I_o' \, . \tag{38}$$

That is, if the divergence of the light waves is two orders of magnitude broader than the natural diffraction latitude $g(\beta)$, the probability of electron reflection is depressed two orders of magnitude below the maximum probability P_μ for the given light intensity. A not insignificant compensation for this disadvantage, however, is that the problem of aligning the electron beam with respect to the light beam may be two orders of magnitude easier.

Bragg planes with non-uniform densities

In the above sections we have dealt with light waves which were considered to have featureless wave fronts. Standing waves in a laser cavity, however, as a rule possess nodal surfaces parallel to the laser axis in addition to the principal nodal planes perpendicular to the axis. The mathematical modification required to treat such a case is self-evident; it simply involves a modification of the form of $V(\vec{r})$ to be inserted into Equation 8. Since the forms encountered in typical high power lasers are complex and irregular it does not seem profitable at present to give details of integration for non-uniform densities of wave fronts. Nevertheless, it is worthwhile to discuss one aspect of axial nodes.

A standing wave in an ideal cavity with a rectangular cross section has a periodicity in three rather than just one dimension. The principal planes are populated, then, with "atoms" of localized photon density in a regular array. Families of Bragg planes can be constructed to pass through these "atoms" in many different directions. As a consequence, it is possible to satisfy the Bragg condition by certain planes which are tilted with respect to the principal planes. The allowed reflections, according to an analysis of Equation 8, are from planes in which the Miller indices are zero or unity. Since the wave length perpendicular to the axis of a standing wave is extremely large compared with the wave length along the axis, the total angle of electron scattering is virtually the same for 001, 011, 101, and 111 reflections.

The existence of the nodes parallel to the laser axis signifies, of course, that the photons have a non-zero component of momentum perpendicular to the axis. Indeed, in a cavity b units across spanned by n transverse waves, we may consider the standing wave to be generated by criss-crossing running waves slanting off axis be a definite angle $\pm \eta_b$ where

$$\eta_b \simeq \lambda_p n_\eta / b .$$

For a ruby laser with b = 1 centimeters and $n_\eta \simeq 50$, the value of η_b is about three milliradians, a not atypical value. A point to note, however, is that if the standing wave consists of a single such mode it is inappropriate to invoke Equation 37 just because the output exhibits a divergence. Even though slant η may be enormous compared with the breadth of $g(\beta)$, the electron reflection probability is undiluted by the light divergence if the light is fully coherent. Allowed reflection

angles are not spread over a continuous range of β_o as they are in the previous section; they are concentrated sharply in the allowed Bragg reflections. The principal (001) reflection for our ideal single divergent mode case (rectangular cross section) is as intense as that for a non-divergent mode of the same photon intensity. The higher index (101, $\bar{1}$01) reflections are tilted by β_o values of $\pm \eta_b$ and are one-fourth as intense.

Calculation of probabilities for stimulated Compton scattering

Table 1 gives numerical results for interaction probabilities of stimulated Compton scattering for a variety of different laboratory conditions.

Table 1. Stimulated Compton scattering probabilities for various laser intensities, wavelength spreads and divergences. Assume laser wavelength as 6900 Å, assume 1.65 Kv electrons, and let ℓ be 1.2 centimeters.

I_o megawatts per square centimeter	$\Delta\lambda$ Å	divergence radians	$(N/N_o)_{max}$
10	≤ 0.006	0	0.25
10	$\ll 0.6$	3×10^{-3}	0.0025
100	$\ll 0.6$	3×10^{-3}	~ 0.25
100	< 0.6	$\ll 3 \times 10^{-3}$	~ 0.25
140	$\ll 0.6$	1×10^{-2}	~ 0.4
55[a]	0.02	4×10^{-3}	0.07

[a]represents idealized laboratory conditions with a uniform distribution of laser powers

EXPERIMENTAL

Apparatus

An electron diffraction unit has been constructed to investigate stimulated Compton scattering. The detection of stimulated Compton scattering involves formidable obstacles. Below is a list of specifications and requirements which were considered in designing the apparatus.

(a) It was decided in early stages of the investigation that medium energy electrons (1640 volts) would be used in conjunction with a high powered ruby laser with a characteristic output of 6943 Å. Slower electrons are more difficult to produce and control with precision, and faster electrons exhibit smaller Compton recoils.

(b) The expected total scattering angle for stimulated Compton scattering is 8.7×10^{-5} radians. The electron detector must be able to measure small scattering angles.

(c) An electron source needs to be designed with suitable lenses and deflectors to collimate electrons. Preferably, the electron beam should be parallel to a fraction of a milliradian when it intersects the laser beam. The system must be capable of focusing the electron beam to less than 8.7×10^{-5} radians for detection.

(d) The laser axis must be mounted perpendicular to the electron beam axis. Success of the experiment depends on adjusting the electron beam to intersect standing light wave planes at the Bragg angle. Laser divergences somewhat liberalize the stringency of this adjustment, but nevertheless, the two beams will need be perpendicular to within 10^{-4} radians.

(e) Probabilities of stimulated Compton scattering will be governed by laser parameters; namely, intensity, divergence and wavelength spread. Conventional laser sources can produce sufficient light intensities only if Q-switching techniques are employed. The duration, however, of these high intensity pulses is only 10-20 nanoseconds.

(f) The short time of laser action will necessitate either a very high electron beam intensity or an electron detector system to observe small numbers of deflected electrons.

(g) To obtain the high resolutions required, the electron beam must be shielded from magnetic fields. This includes the earth's magnetic field. The greatest difficulty, however, involves shielding the electron beam from the huge flash-lamp pulse when the laser is fired.

Each component of the apparatus will be treated in more detail in the following sections. In most cases, only the final model of electron diffraction unit will be discussed.

Electron gun, lenses, and deflectors

Figure 3 and Figure 4 are front and rear photographs of the electron diffraction unit. A 10 inch rectangular brass box supported cylindrical tubes extending above and below the box. The box also supported the laser and introduced laser radiation whereby it intersected the electron beam. Electrostatic lenses, with high resolution in one direction, and deflectors were contained in the brass cylinders. A plate closing the upper cylinder supported the electron gun, a plate closing the lower cylinder supported the electron detector. The entire unit was evacuated with a six inch diffusion pump which, with the aid of a cold trap at

Figure 3.   Front-view photograph of the electron diffraction
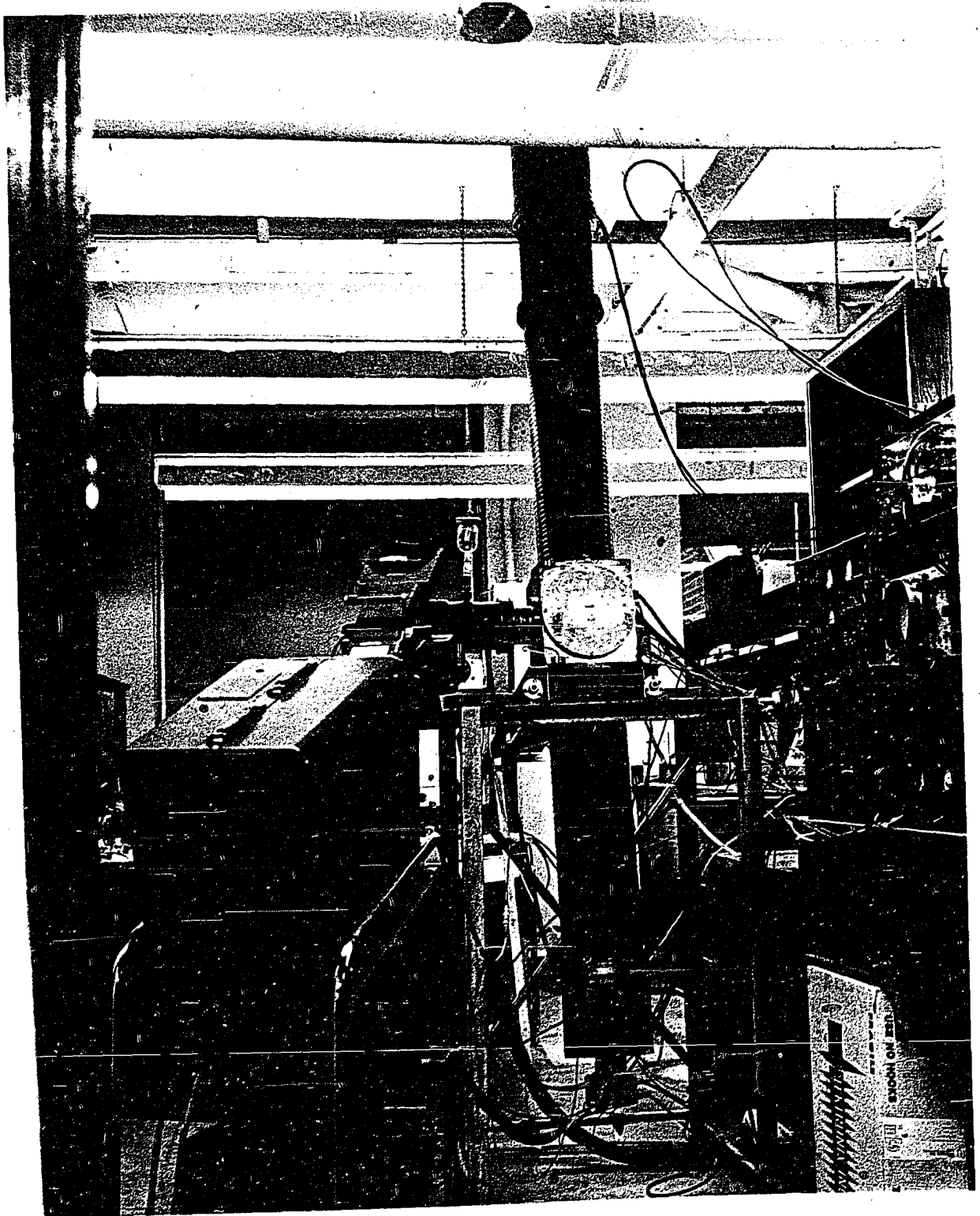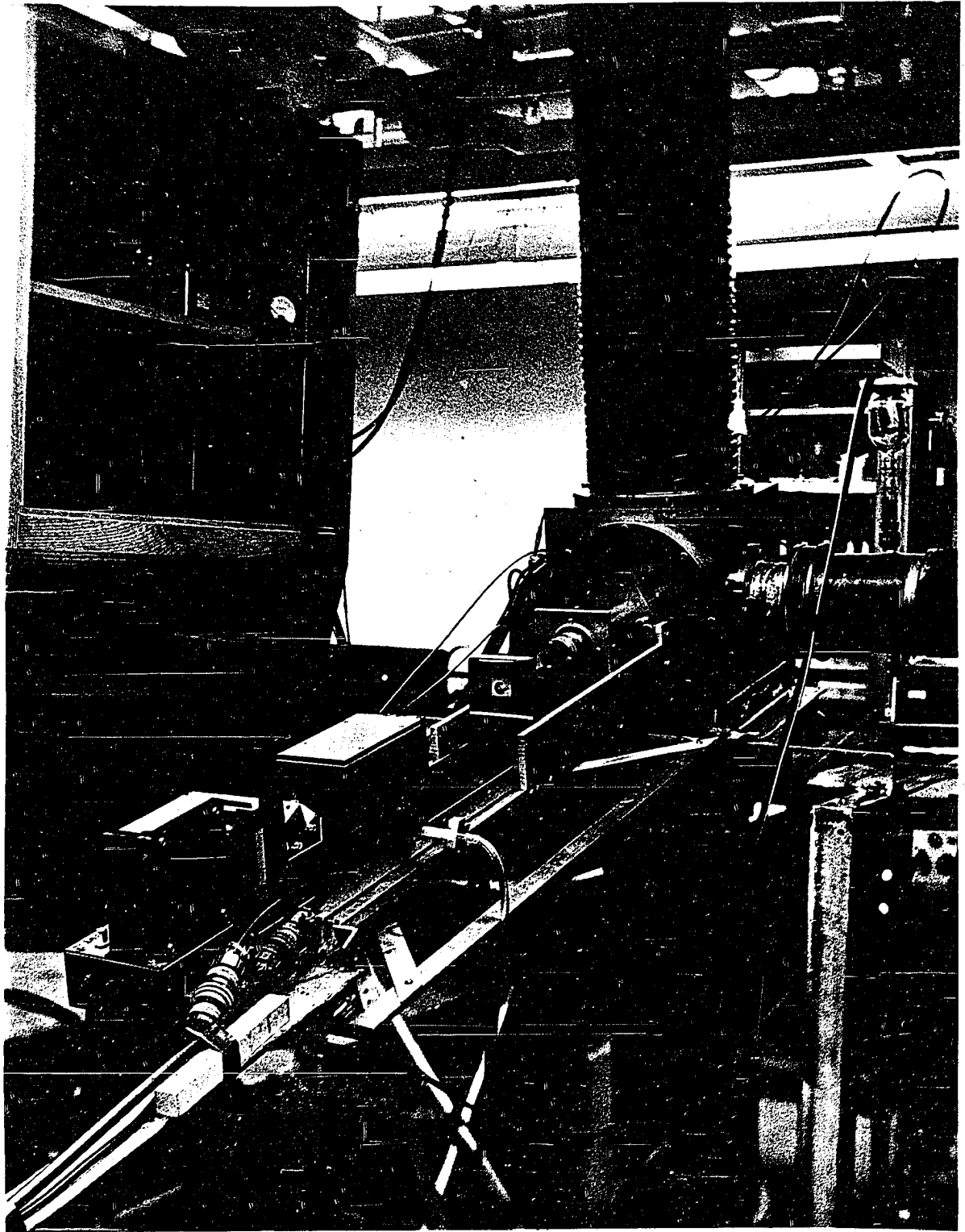   unit used to measure stimulated Compton scattering

Figure 4. Rear-view photograph of the electron diffraction
unit used to measure stimulated Compton scattering.

liquid nitrogen temperatures, maintained a pressure of 10^{-6} millimeters of mercury.

An electron gun, as shown in Figure 5a. was patterned after one used in a conventional gas electron diffraction unit. An RCA electron microscope filament was mounted 0.21 centimeters from a grid cup. Electrons left the filament, which was heated by 2 amperes from a 2 volt direct current source, and were accelerated through a potential difference of 1640 volts. The electron gun was self-biased as illustrated in Figure 6, and was operated at a space current of 50 microamperes.

Lenses, deflectors and apertures allowed a versatile manipulation of the electron beam. Figure 7 identifies the placement of lenses and deflectors, shows the lens type at any position along with the function each lens is to perform, and schematically illustrates the path electrons traverse from electron gun to electron detector. Lenses are identified by arabic numerals beginning with 1 on top and progressing through 6 on the bottom. Additional information on lens dimensions, aperture spacings, focal lengths, magnifications, lens purpose and typical applied voltages can be obtained from a brief summary of Table 1. Lens 1 was a demagnifying lens. It took the electron beam cross-over from the gun and produced a much reduced image needed for high resolution. This image became the object which was placed at the focal point of lens 3. Electrons left lens 3 with parallel paths. Lens 4 was identical to lens 3 and was operated at the same voltage as lens 3. Therefore, lens 4 again focused the parallel electrons to give an image above lens 6. Lens 6 magnified the image as well as the scattering angle. Lens 2 and lens 5 were gathering lenses that simply collected electrons which would have

Figure 5a. Cross-sectional view of the electron gun

Figure 5b. Cross-sectional view of the scintillator electron
            detector

FILAMENT
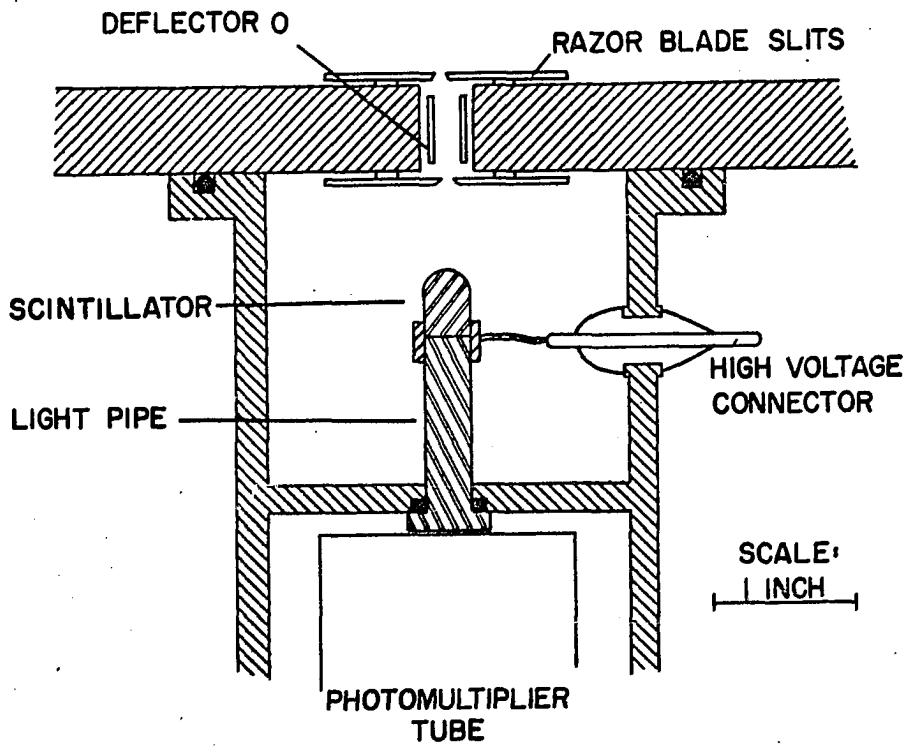
BIAS CUP

GLASS "STAND OFF"

ANODE

DEFLECTOR O

RAZOR BLADE SLITS

SCINTILLATOR

LIGHT PIPE

HIGH VOLTAGE
CONNECTOR

SCALE:
1 INCH

PHOTOMULTIPLIER
TUBE
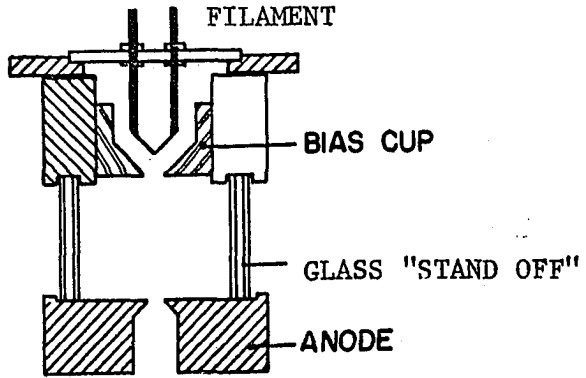
Figure 6. Circuit diagram of self-biased electron gun and of electrostatic lens controls

BRIDGE
RECTIFIER

POWER STAT
TRANSFORMER

2 Ω
25 WATT

2-4000μf
25 VDC

2 VOLTS
FILAMENT

Ⓐ

BIAS
CUP

0.1μf

μA

8μf
2000 VDC

100 K

100 K

LENS 1

LENS 2

LENS 3-4

LENS 5

LENS 6

mA

470K   470K

88 MEG

8μf
2000 VDC

I MEG.
2 WATT
EACH

250K
EACH

INPUT 0-1650 V
FROM REGULATED
POWER SUPPLY

34
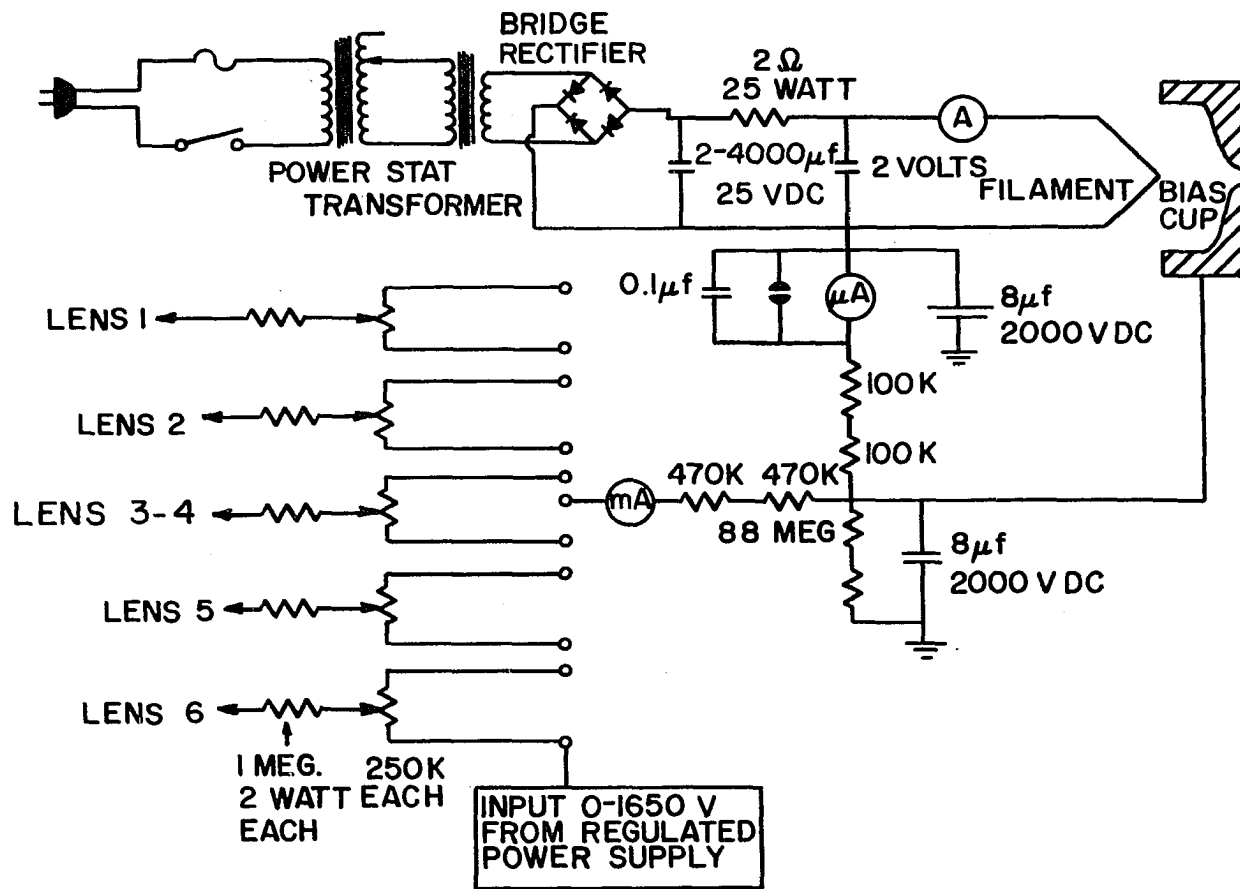
Figure 7. Schematic diagram of the electron optics in the
electron diffraction unit

ELECTRON GUN

DEMAGNIFICATION — LENS 1

DEFLECTOR 1

LENS 2 — GATHERING

DEFECTOR 2

COLLIMATION — LENS 3

SCALE - 10"

LASER ASSEMBLY

INTERACTION CAVITY

COLLIMATION — LENS 4

DEFLECTOR 4

LENS 5 — GATHERING

DEFLECTOR 5

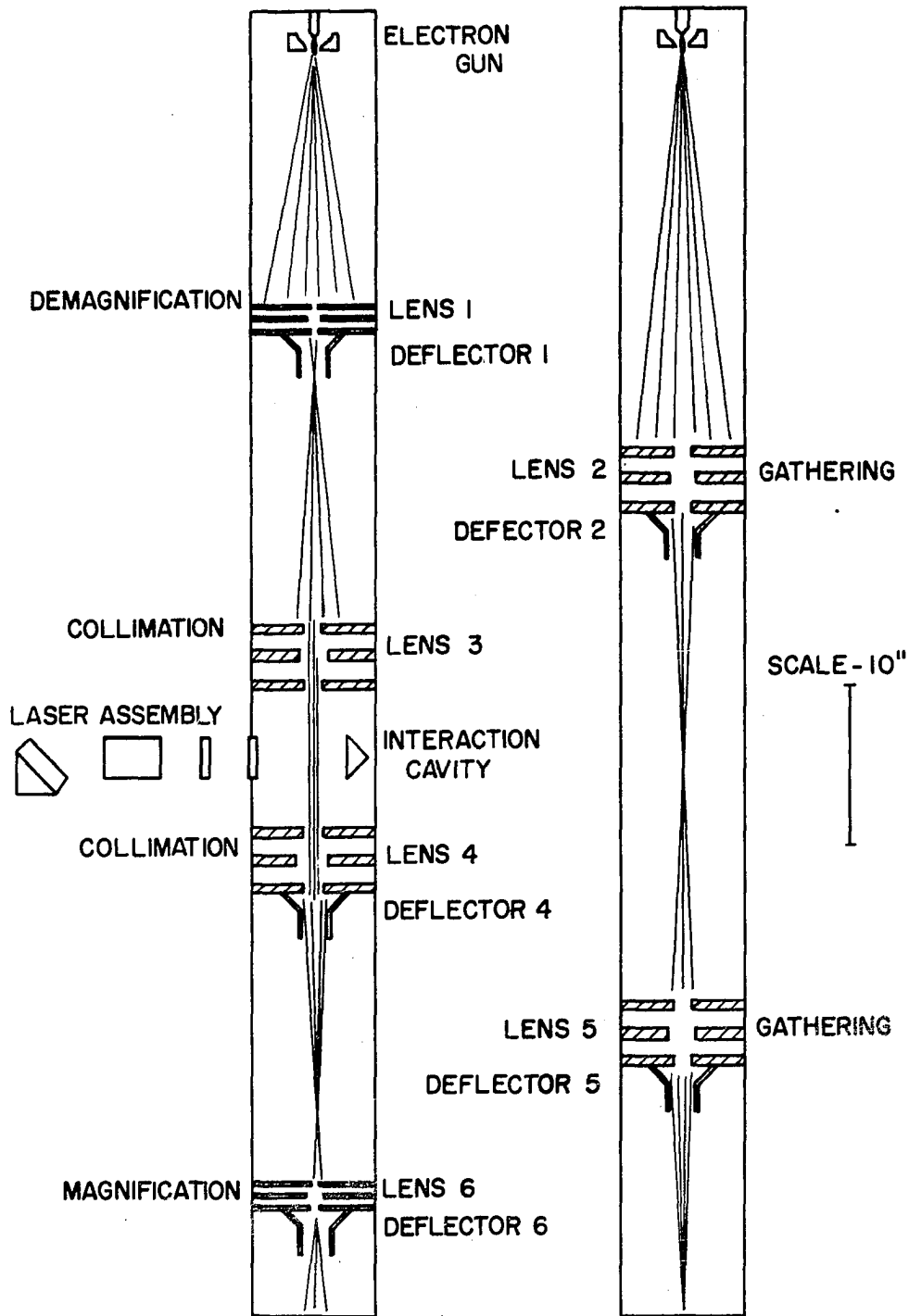MAGNIFICATION — LENS 6

DEFLECTOR 6

Table 2. Information concerning lens dimensions, aperture spacings, focal lengths, magnifications, and applied voltages

	A[a] inches	B inches	C inches	D inches	E inches	Purpose	Magnification	Focal length inches	Typical voltage
Lens 1	0.03	0.134	0.35	0.78	0.28	demagnification	1/14	0.5[b]	1650
Lens 2	0.63	1.125	2.31	1.31	1.13	gathering	----	17.	1260
Lens 3	0.63	1.125	2.66	----[c]	1.13	collimating	----	20.	1070
Lens 4	0.63	1.125	2.66	1.25	1.13	collimating	----	20.	1070
Lens 5	0.63	1.125	2.31	1.31	1.13	gathering	----	17.	----[d]
Lens 6	0.50	0.134	0.35	0.78	0.28	magnification	14	0.5	1650

[a]See Figure 8 for definition of A, B, C, D, and E

[b]Focal lengths are only approximate values

[c]No electrostatic deflector on lens 3

[d]Lens 5 was rarely used

37

ordinarily been lost. Lens 5 was, however, rarely used because electron beam inhomogeneities contributed to poor electron beam focus. All six lenses used in the unit were unipotential, 3-aperture planar lenses. One set of lenses, the magnifying or demagnifying lenses, contained small, closely spaced apertures, and possessed short focal lengths. Lens 1 was demagnifying and lens 6 was magnifying. The larger lenses or gathering and collimating lenses, were designed to have long focal lengths and low magnifications. Lenses 2, 3, 4, and 5 were in this group. Figure 8 gives a scaled cross-sectional view of the larger model of lens used. By comparing actual photographs of Figure 9 and Figure 10, the similarities and differences between the two models can be readily observed. The two models were alike in the following respects. Each had three apertures with the central adjustable aperture maintained at a variable voltage between zero and 1640 volts. Top and bottom apertures were identical in size and kept at ground potential. Each lens, with the exception of lens 3, was equipped with a set of equal potential deflection plates to control the electron beam. Adjustable copper, knife-edge apertures on the top side of each lens masked stray or "fuzzy" electrons. Figure 11 shows the regulated high voltage supply which was used to operate the electrostatic lenses and electron gun. Figure 12 presents a circuit diagram of the deflection system.

Magnetic fields in vicinity of the electron diffraction unit severely impaired electron beam focus. For this reason, a great deal of care was taken to control or eliminate magnetic fields. First, a room was selected as free as possible from metal cabinets and fixtures and which was not close to heavy electrical equipment. Whenever possible, raw

Figure 8. Cross-sectional view of unipotential, three-
           aperture, electrostatic lens

SCALE-2"

A

APERTURE

B

GROUND
POTENTIAL

C

NEGATIVE
POTENTIAL

E

D

GROUND
POTENTIAL

DEFLECTORS
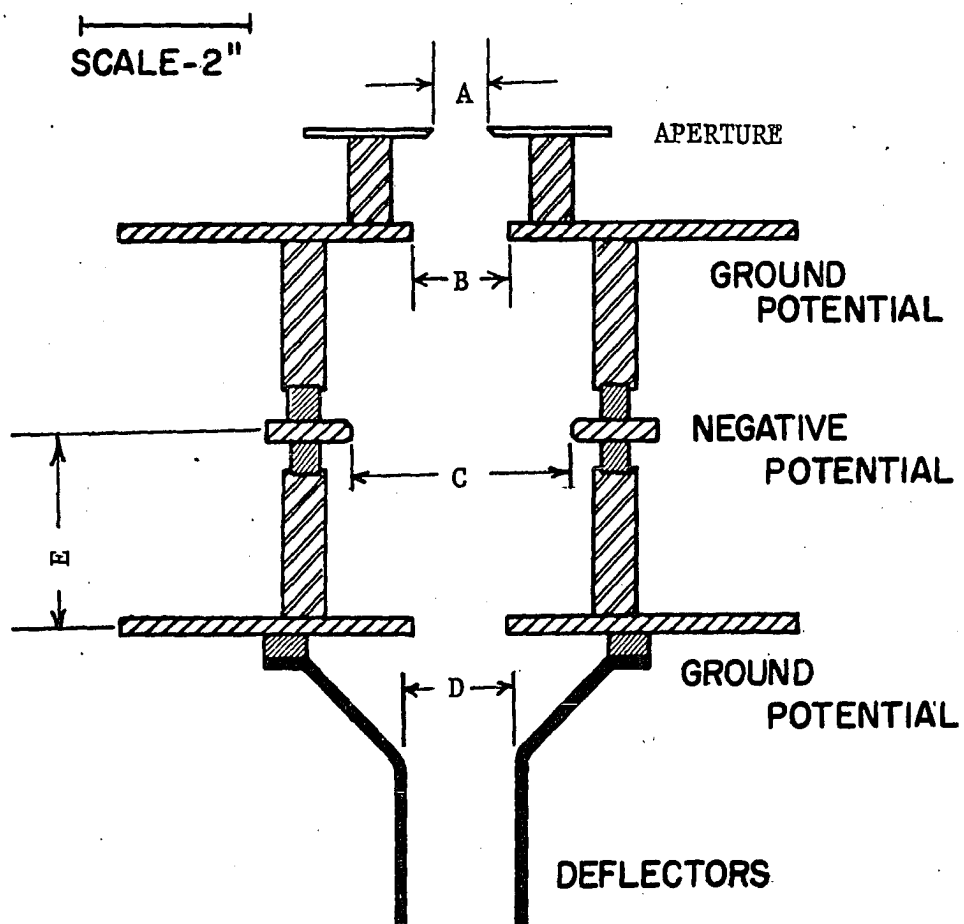
STAINLESS STEEL
BAKELITE
ALUMINUM
COPPER

Figure 9. Photograph of large electrostatic lens
used for electron collimation
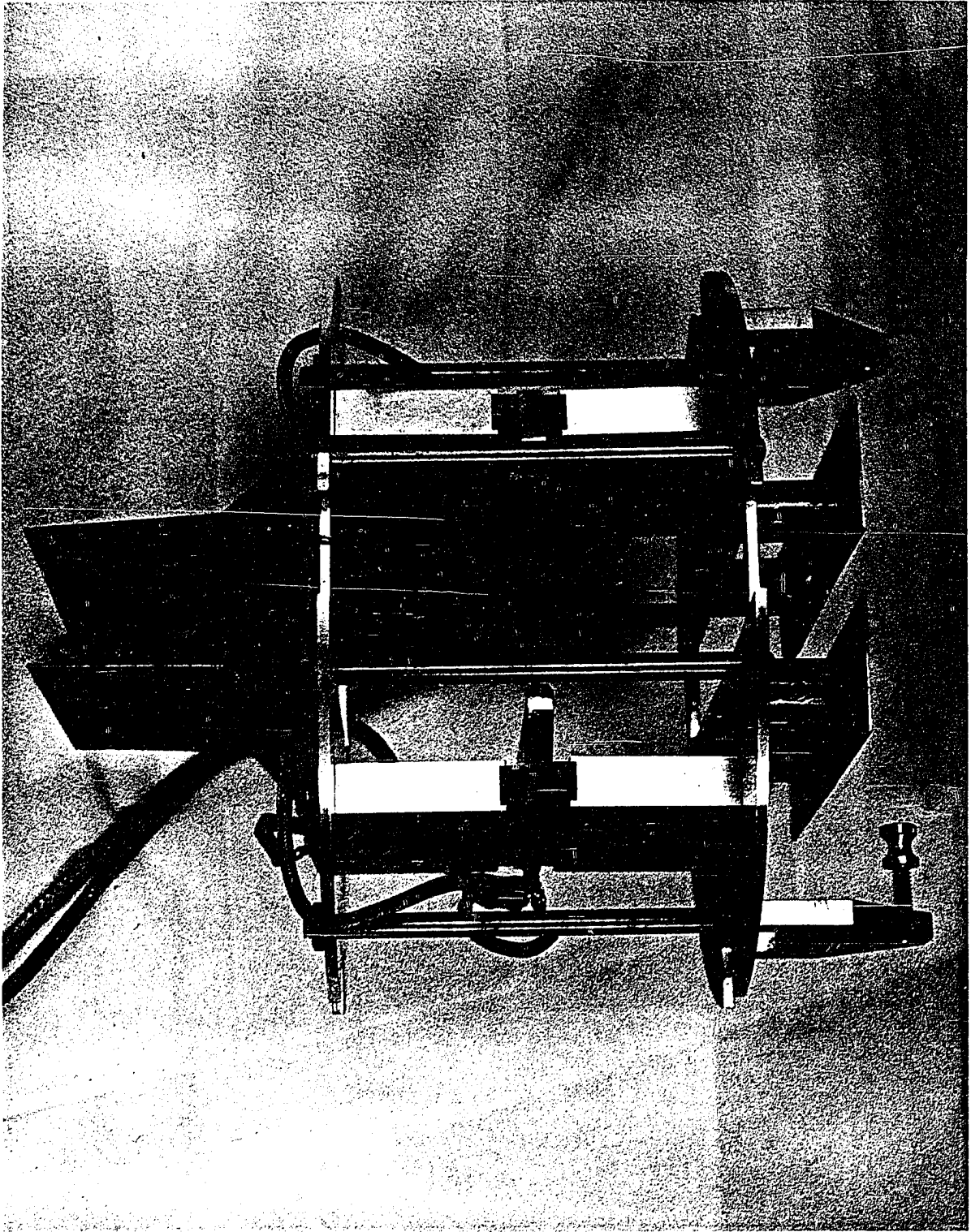
Figure 10. Photograph of small electrostatic lens
            with a large magnification
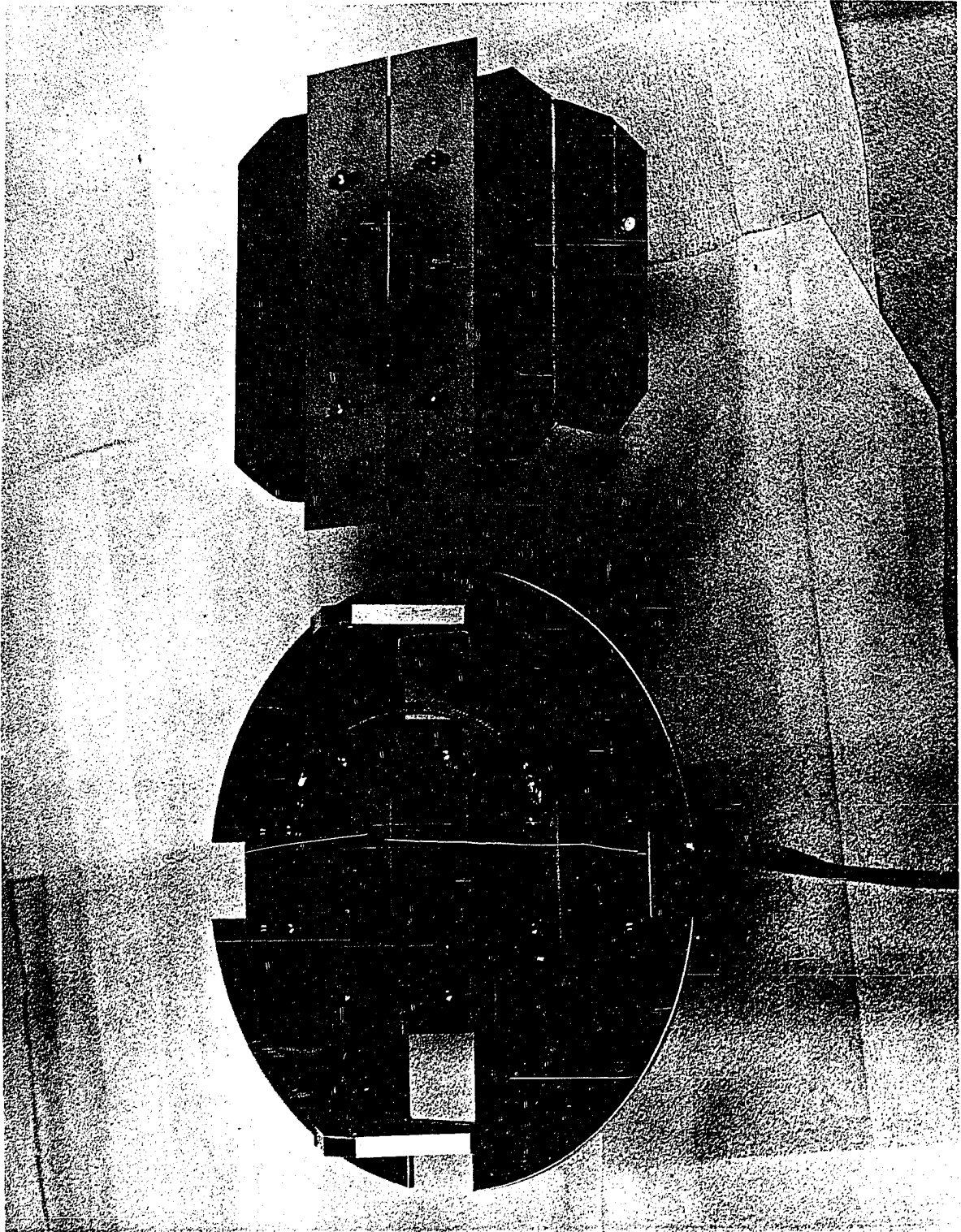
Figure 11. Regulated high voltage power supply to operate
electron gun and electrostatic lenses

STANCOR
P8151

O VOLTS

2400V

2.5 V

2X2

-2800V

0.1μf 5kv

0.1μf 5kv

22K 2 WATT

26K

26K

66K

4.7 MEG 2 WATT

4.7MEG

4.7 MEG

4.7 MEG

-2330 V

180 K 0.6 MA

180 K 0.5 MA

-1600V

12AX7

+ 90V

-1730 V

120K 2 WATT

-1500 V

1.2 MEG 1 WATT

250K

-1870V

2.2 MEG 1 WATT

807

STRING OF 11-VR150

O VOLTS

OD3 VR150 -150 VOLTS

OD3 VR150 -300 VOLTS

OD3 VR150

-1650 VOLTS

18 K 5MA

-1740 VOLTS

OD3 VR150

-1860 V

2-47K 2 WATT 0.5 MA
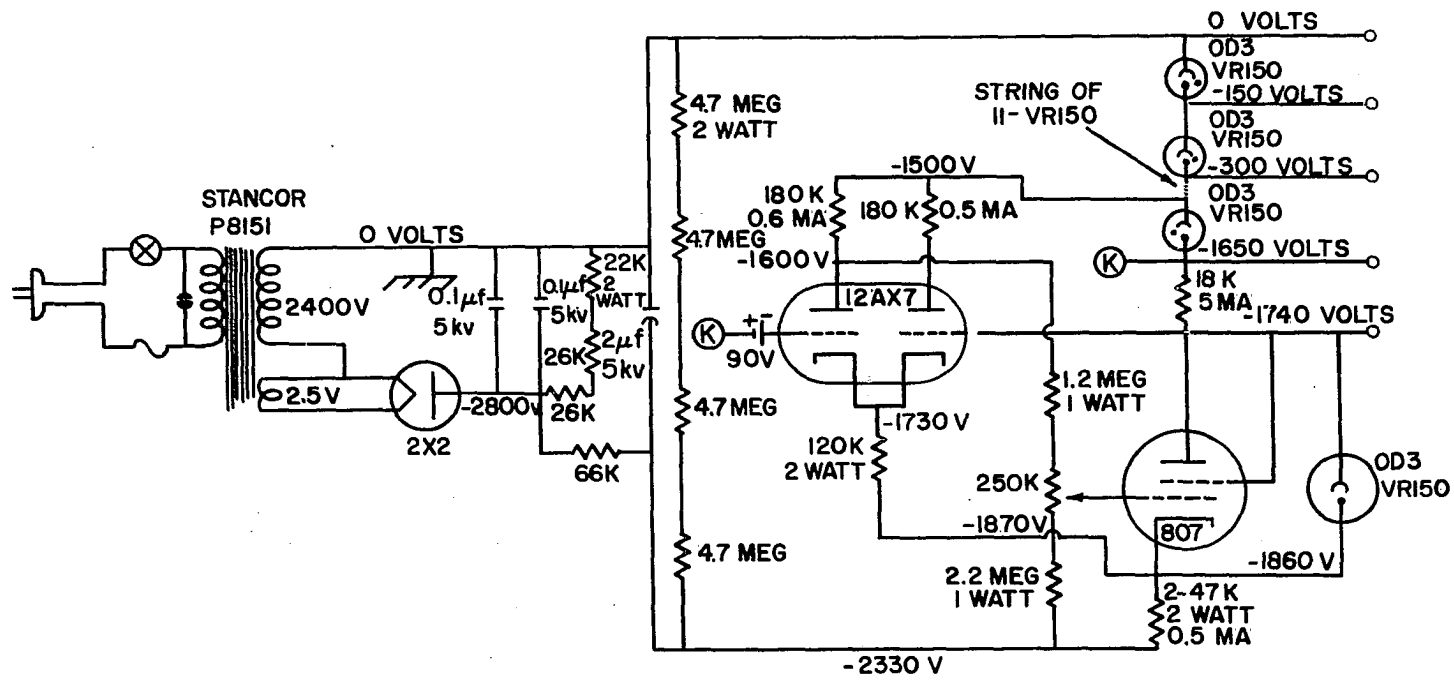
Figure 12. Circuit diagram of the deflector system controls

DEFECTOR O

DEFLECTOR I

DEFLECTOR 2

DEFLECTOR 5

DEFLECTOR 4

DEFLECTOR 6

DEFLECTOR DUAL POTS
EACH 250 K

+180 V.
-180 V.

100K
100K

I MEG   I MEG

I MEG   I MEG.

330K   330K

INPUT ELECTRON
SWEEP SIGNAL

1.35 V   1K
CALIBRATED
PUSH-BUTTON

+270 V.

100K
100K
100K
100K
100K

I MEG

I MEG

-270 V.

6.3 V.
A.C.

1K
2.5μf

10 K DUAL POT

100K
100K
100K

0.25μf
0.25μf   100K   100K

1K
2.5μf

10K DUAL POT
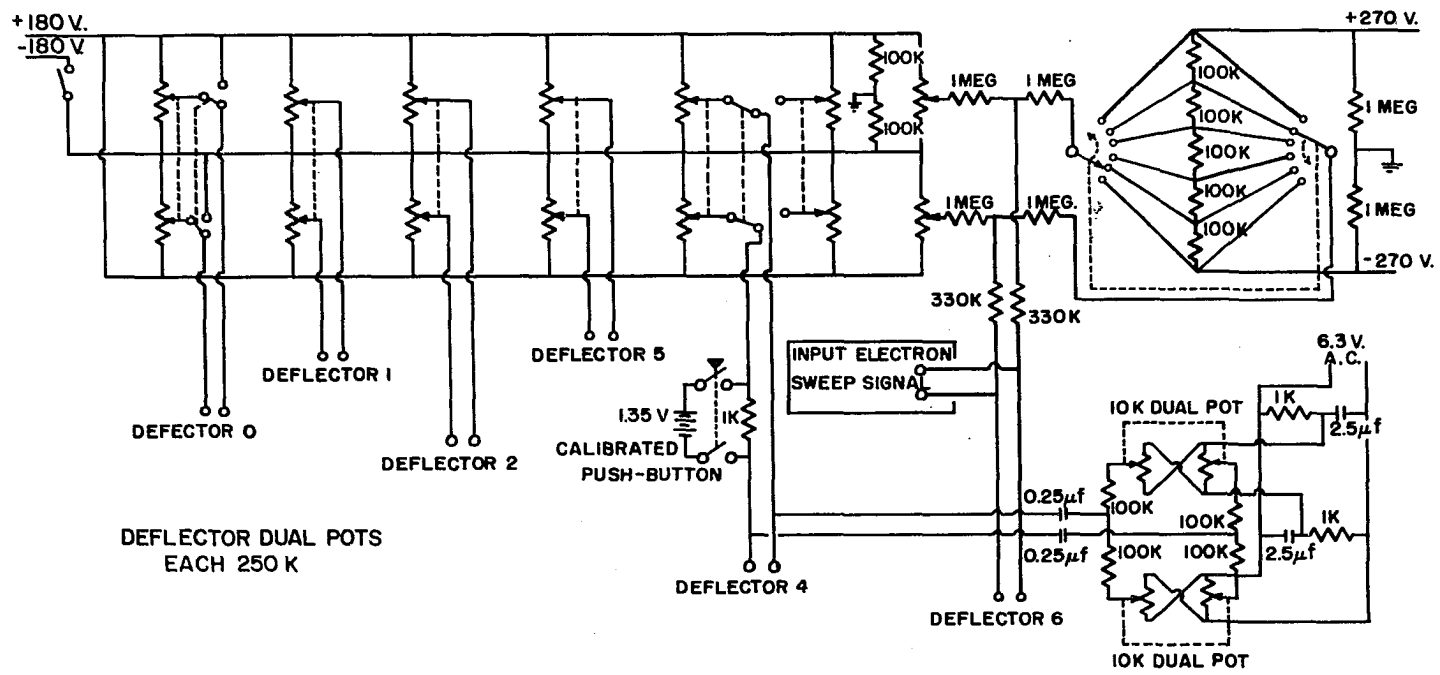
materials for construction of unit and all accessories were of either

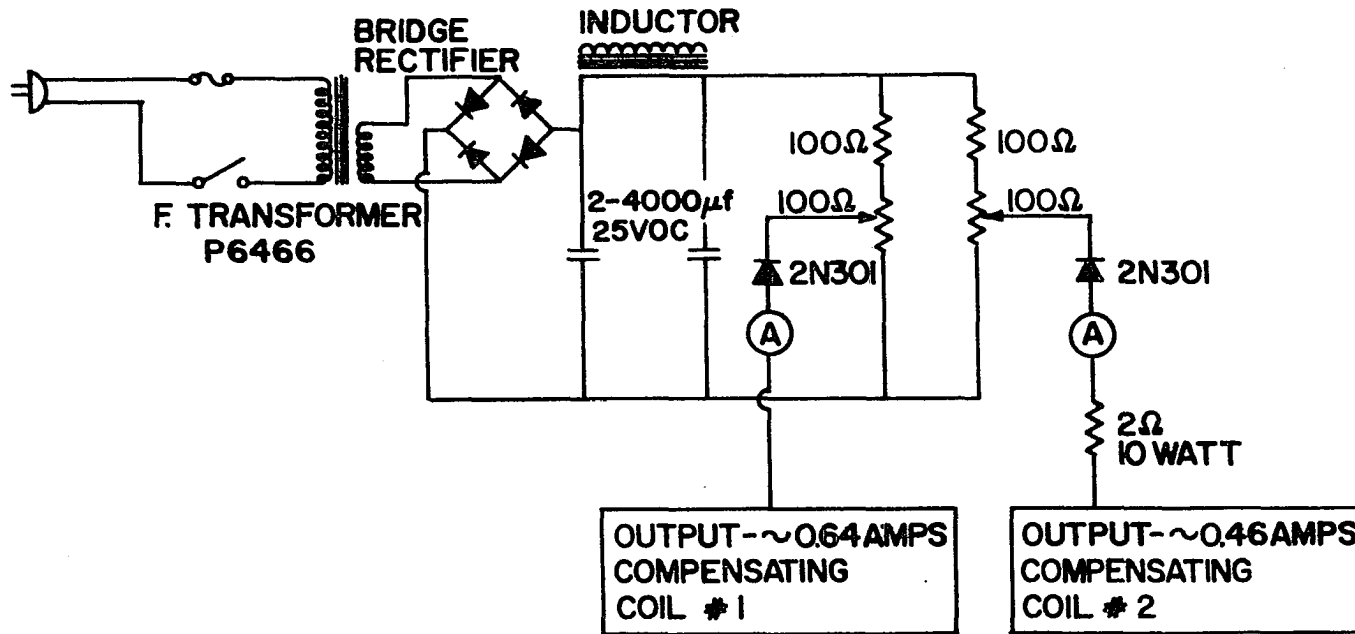brass, aluminum, copper, or stainless steel, but some magnetic components

had to be tolerated. Transformers built into electical and electonic

panels were bothersome, but in most cases, could be shielded or removed

to safe distances from the unit. The earth's magnetic field also disturbed

1640 volt electrons traversing the 85 inch path. The earth's magnetic

lines of force were found to be tilted 10 degrees from vertical. There-

fore, the entire unit was tilted so that the electron beam followed the

magnetic lines of force. A magnetic coil was wound on the lens cylinders

of the unit. Figure 3 and Figure 4 show the coils which were covered

with black electrical tape to hold the coils in place. The noncylin-

drical center block was equipped with an internal coil. Also, coils were

extended beyond the lens cylinders by adding cylindrical extensions as

supports for additional coil. With a coil density of about 1.7 turns

per inch, and a coil current in the proper direction of about 0.6 amperes,

the earth's magnetic field inside the unit was virtually cancelled.

Gaussmeter probes aided in adjusting coil densities along the lens tubes.

Magnetic fields inside the unit varied between zero and 0.05 gauss as

compared to the normal earth's field of about 0.5 gauss. Figure 13 gives

the circuit diagram of a power supply used to furnish compensating coil

currents.

Electron detection system

An electron detector, similar to one proposed by Everhart and

Thornley (6), consisted of a plastic scintillator, a light pipe, and a

photomultiplier. Figure 5b presents the arrangement of components. An

electron beam was admitted to the detector system through a slit which

Figure 13.   Circuit diagram of power supply for
             magnetic compensating coils

BRIDGE
RECTIFIER

INDUCTOR

F. TRANSFORMER
P6466

2-4000μf
25VOC

100Ω

100Ω

100Ω

100Ω

2N301

2N301

Ⓐ

Ⓐ

2Ω
10 WATT

OUTPUT-~0.64AMPS
COMPENSATING
COIL #1

OUTPUT-~0.46AMPS
COMPENSATING
COIL #2

was 0.005 inches wide and was outlined by two stainless steel razor
blades. A lower slit was somewhat offset, and electron gun filament
light was excluded from the detector. Deflector 0, however, directed
electrons through the second or lower slit. The scintillator, an Ne
102 plastic phosphor obtained from Nuclear Enterprises Ltd. of Winnepeg,
Canada, was coated with a 500 Å thick aluminum film. This coating
served several purposes. First, a positive electron accelerating po-
tential of 20 kilovolts was applied to the scintillator film. Electrons
passed through the aluminum and upon striking phosphor, caused emission
of visible radiation. The aluminum film also acted as a mirror to direct
visible radiation toward a light pipe which conducted radiation to an
RCA 6655A photomultiplier. Output signals, with a load resistor of 10 K
ohms, were coupled to a cathode follower. Finally, cathode signals were
monitored with a carefully tuned oscilloscope probe and Tektronix 551
oscilloscope with a type L plug-in amplifier. Figure 14 gives more de-
tail concerning electrical circuits.

Electron scattering angles were measured by scanning the beam past
the scintillator detection slit. If the slit was small enough, deflected
electrons were observed at a different time from undeflected electrons.
A sawtooth signal applied to deflector 6 was responsible for executing
the scan process. Electron beam sweep speed and amplitude were controlled
by adjusting sawtooth voltage and frequency. Figure 15 shows more about
the details of electron detection. To one plate of deflector 6 a posi-
tive sawtooth signal is applied, and to the other, a negative sawtooth
signal is applied. At t_o, before the sawtooth is applied, the electron
beam is near the right edge of the slit in a position controlled by a

Figure 14. Circuit diagram and schematic of photomultiplier
            power supply, photomultiplier, and cathode follower
            used to measure scintillator response to electrons
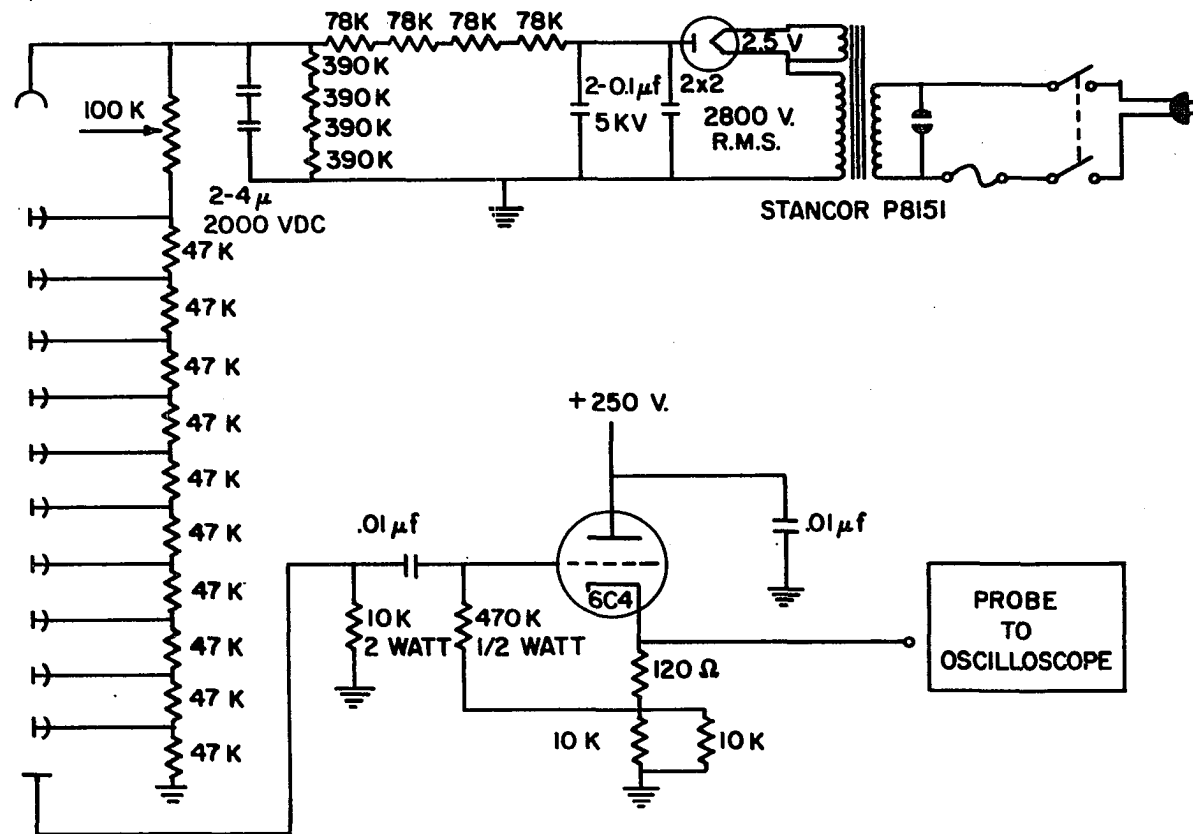
Figure 15. Schematic diagram of the major components in the electron diffraction unit and the methods of obtaining data

ELECTRON GUN

LENS

LASER ASSEMBLY

PHOTOMULTIPLIER

t_0 t_1 t_2 t_3

POSITIVE
SAW-TOOTH
SIGNAL

DEFLECTORS

t_0 t_1 t_2 t_3

NEGATIVE
SAW-TOOTH
SIGNAL

ELECTRON PATH AT t_0

SLIT
SCINTILLATOR
LIGHT PIPE

PHOTOMULTIPLIER

PHOTOMULTIPIER

V_2

V_3

V_1

LASER POWER
DETECTOR

LASER ENERGY
DETECTOR

ELECTRON
DETECTOR

t_0 t_1 t_2 t_3

56
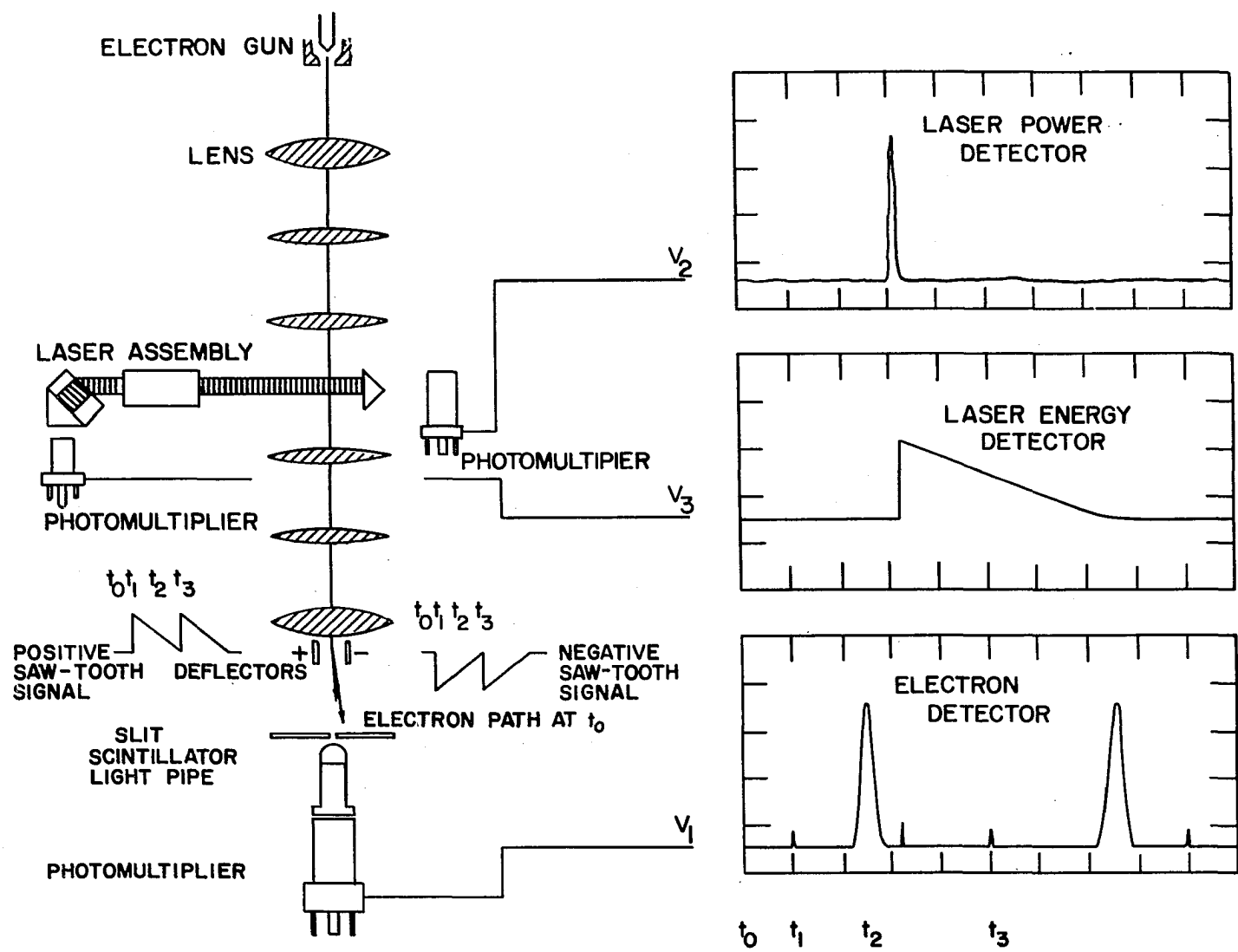
direct current voltage applied to deflector 6. Let us consider that the sawtooth voltage is applied at time t_1, rapidly sweeping the electron beam past the detection slit. The oscilloscope response shows a short pulse which we shall call a "fly back". As the sawtooth voltages decrease linearly back to zero, the electron beam reverses its sweep and drifts linearly back to its original position on the right of the slit. At t_2 the beam passes through the slit and produces a large pulse on the oscilloscope. Time t_3 marks the start of another sweep cycle.
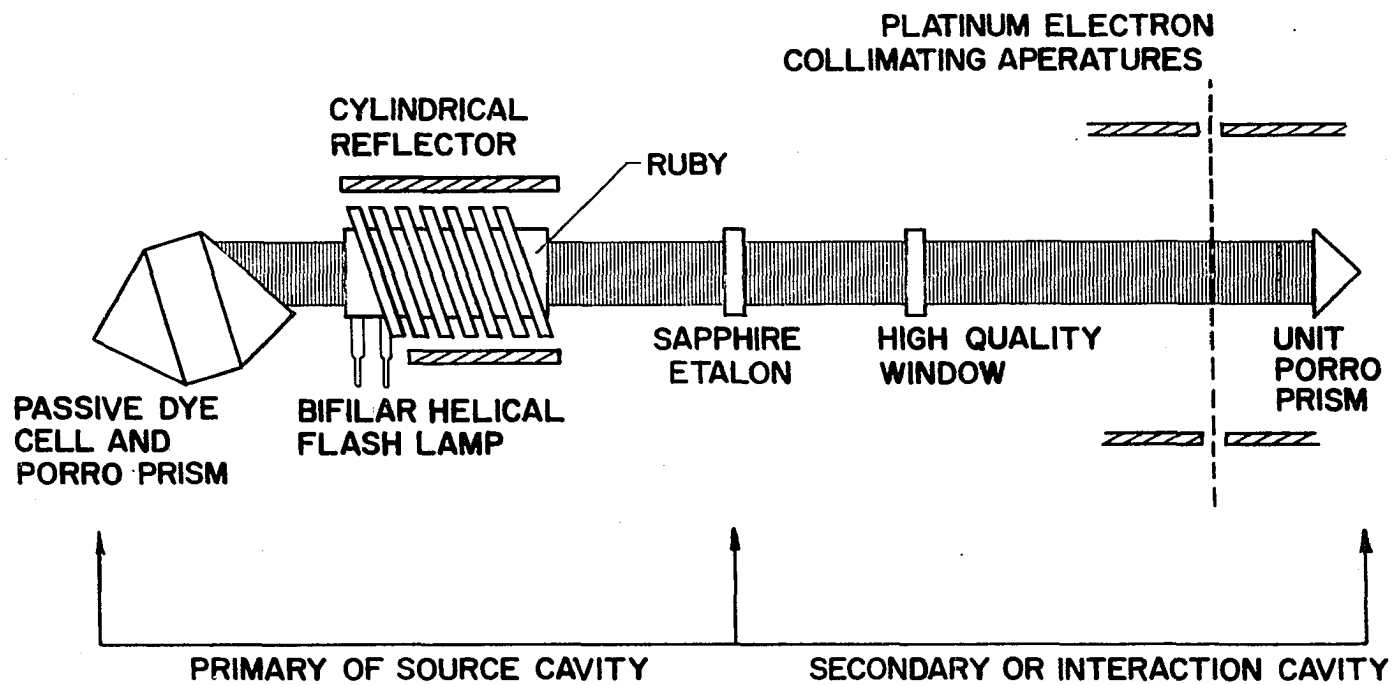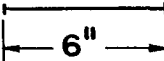
Laser

A ruby laser, the Korad K-1 model, was used in this investigation. The ruby rod was 7/16 of an inch in diameter and four inches long and was pumped by a Kemlite bifilar helical flash lamp. Originally, the laser was operated in a conventional mode with simple dielectric mirrors to define the cavity. Typical outputs consisted of approximately 200 separate spikes, each of which had a duration of about one microsecond. According to Korad specifications, the total burst energy of about 24 joules gives peak powers of the individual spikes of about 0.25 megawatts. Simple calculations show that higher laser powers are required to obtain stimulated Compton scattering probabilities greater than, say, four per cent. In our system, when it was found that individual electron noise events gave signals of about two to four per cent of the electron beam signal, it became evident that a higher laser power was needed than could be obtained with normal burst mode operation. For this reason, a passive dye cell was purchased from the Korad Corporation to make it possible to generate giant pulses. The dye cell assembly was

composed of a Brewster angle window, a compartment for saturable dye

solutions, and a totally reflecting porro prism. High flux radiations

from Q-switched laser operation dictated the use of porro prism reflec-

tors as opposed to coated mirrors which are damaged in a single giant

pulse. A dilute solution of cryptocyanine dye in methanol (7, 8) is

placed into the passive cell to suppress laser emission until a high

energy inversion is obtained. Ultimately, saturation of the dye is a-

chieved and the solution becomes transparent to the laser radiation.

At this point an intense laser action takes place. If the dye concen-

tration is correct, a single giant pulse can be obtained. The giant

pulses obtained in the present investigation had energies of 0.8 to 1.0

joules and lasted about 10 to 20 nanoseconds. Peak powers of 80 mega-

watts were frequently obtained.

The laser arrangement in the experiment was unusual. Figure 16

illustrates schematically the arrangement of pertinent laser components,

and the photograph in Figure 4 may be helpful in clarifying the labora-

tory arrangement. Conventional lasers are equipped with one totally

reflecting mirror and one partially transmitting mirror. The cavity

losses by transmission through the latter mirror usually constitute the

useful output of the laser. In the present study, however, a second

porro prism was added to reflect the output of the partially transmit-

ting mirror. As a result, the laser action is governed by the complex

interplay of the two coupled resonant cavities. Since the extreme

boundaries of the laser cavities were totally reflecting prisms, the

only losses from the cavity were the result of beam divergences. These

losses were considerable, however, because of the great length of the

Figure 16. Schematic diagram showing the arrangement of
laser components

PLATINUM ELECTRON
COLLIMATING APERATURES

CYLINDRICAL
REFLECTOR

RUBY

PASSIVE DYE
CELL AND
PORRO PRISM

BIFILAR HELICAL
FLASH LAMP

SAPPHIRE
ETALON

HIGH QUALITY
WINDOW

UNIT
PORRO
PRISM

60

PRIMARY OF SOURCE CAVITY

SECONDARY OR INTERACTION CAVITY

SCALE

6"

great length of the cavities. Actually, the two cavity system somewhat enhanced laser laser energy and laser power over the conventional short cavity arrangement. This was fortunate because a long cavity was needed, as explained below, and conventional long cavities usually give appreciably lower powers than short cavities.

The final laser arrangement was a compromise of several factors. The first flashlamp used was a simple helical inert gas flash lamp. When 25 amperes of current was discharged through the coiled flash lamp, the resulting magnetic field greatly disturbed the electron beam. For this reason, the standard flashlamp was replaced by a specially constructed bifilar helical flash lamp in which the helix returned on itself and cancelled out most of the magnetic field. If a reasonable distance was maintained between flash lamp and electron beam, the residual magnetic disturbance on the electron beam could be reduced to tolerable limits. Even the position of power cables extending from the laser head to a power panel ten feet away was extremely critical.

For acceptable laser performance, all the optical components had to be aligned for parallelness. The intermediate sapphire resonant reflector was not essential for obtaining laser action. Its most important function was to serve as a reference surface with respect to which all other components could be aligned. No other surface in the cavity was in a position to satisfy this need.

Triggering and synchronization.

Electronic circuits helped circumvent several problems. Initial difficulties will be presented briefly, and the circuits used to remedy

various situations will be summarized. Detailed circuit diagrams appear in Figures 17 through 24. Figure 25, on the other hand, schematically illustrates the essential points.

The electrical circuits possessed a characteristic 60 cycle disturbance. Electrical filters removed nearly all of the 60 cycle signal from direct current power supplies, but small residual alternating signals remained to influence the electron beam. Since an extraordinary resolving power was needed in the experiment, the disturbances had to be overcome. The greatest disturbances occurred in compensating magnetic coil current, electron gun filament current, and the high voltage source for both electron accelerating voltage and electrostatic lenses. Small perturbations were also apparent from electric motors, fans, and even fluorescent lights. Since all the electrical equipment was powered by the same 60 cycle alternating current line, the net disturbance was also cyclic. Therefore, the best situation was one in which the electron beam was scanned successively past the scintillation detector with the same net alternating disturbance. For example, if the beam sweep was set at once every 1/60th of a second, and each sweep was triggered on a preset phase, the electron beam experienced exactly the same disturbance on each sweep. If the electron beam was swept past the scintillator continuously, the plastic phosphor heated and, as a result, the signals became noisy. For this reason, the production of sawtooth signals for electron detection was controlled so that the electron scanned only several times during a 60 cycle cycle at about 2500 cycles per second. This intermittent electron detection decreased, by an order of magnitude, the number of electrons striking phosphor and also allowed the scintillator to operate at a lower

Figure 17. Phase-adjust amplifier for the triggering
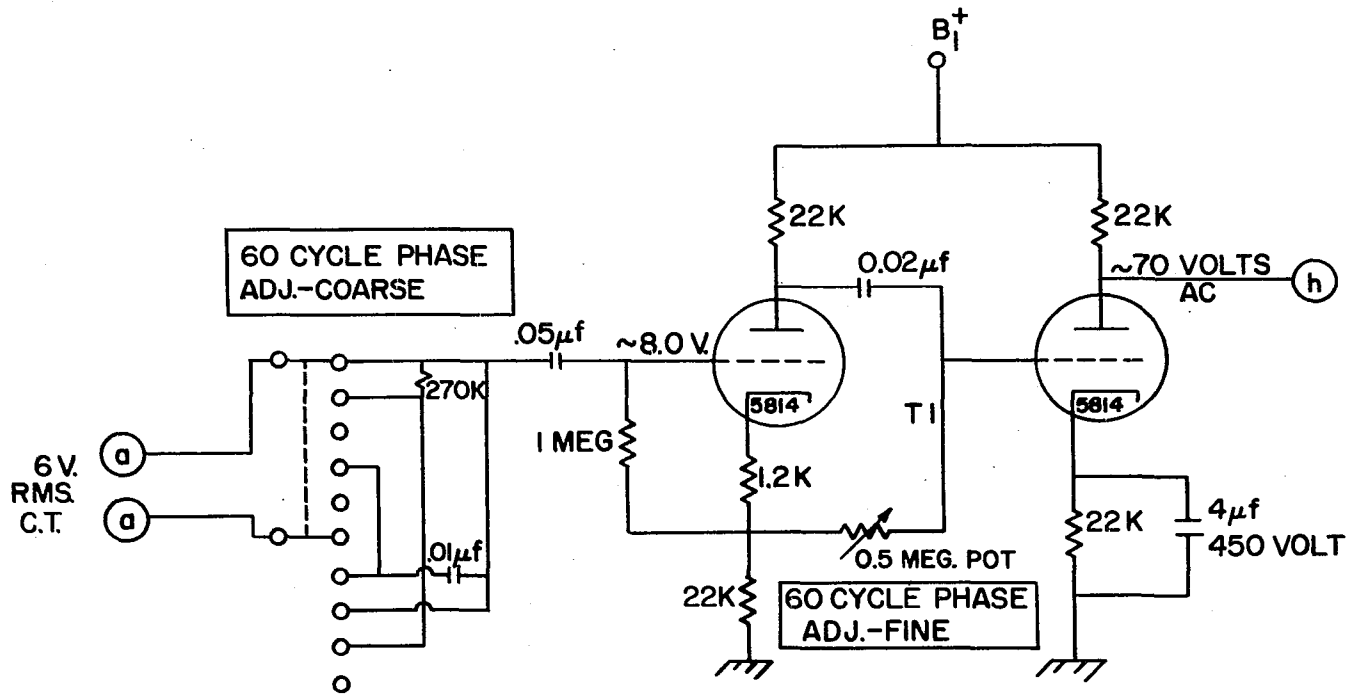and synchronization assembly

Figure 18. Schmidt trigger and sweep control amplifier of the
triggering and synchronization assembly

B_2^+

B_3^+

b

$\frac{1}{60}$ SEC

~70V A.C.

h

.25μf

100K

4.7 K 2W

4.7 K 2W

25μμf

150K

J

.005μf

IN55A

22K

0.1μf

c

180K

15 K 2W

1.5 MEG

MEG POT

280V

.56 MEG

180V

SWEEP CONTROL

100K POT.

47K

6201

T2

6201

10K 2W

100K POT.

68K

c
.01μf
.005μf
.0015μf
600μμf
200μμf

5965

T3

5963

10K 2W

CAPACITOR C SWITCH BY COARSE ON-TIME CONTROL

I MEG POT IS FINE ON-TIME CONTROL

Figure 19. Circuit diagram of sawtooth signal generator
            and amplifier

B_1^+

2.2K

10K

40μf 450 VOLTS

16μf 450V   8μf 450V

10K

1meg POT

680 K

SWEEP CONTROL INPUT ⊙

180 K

470Ω

FREQUENCY RANGE

5963

SWEEP SIGNAL TO DEFLECTOR #6

ADJUSTMENT ON TOP OF CHASIS

20 K

1N55A

100 μμf   300 μμf   780 μμf   .002 μf

5963

884

1K

1K

270 K

AMPLITUDE RANGE SWITCH

1.5K

4.7K

10K

B_1^- B_2^- B_3^-

(-350V)   (-4.5V)

(-12V)

AMPLITUDE CONTROL

5K POT

TRIGGER AMPLITUDE

SCOPE TRIGGER

1.2K

TRIGGER CHOICE

120Ω

TRIGGER INPUT

68

Figure 20. Circuit diagram of the flip-flop trigger of the triggering and synchronization assembly

Figure 21. Trigger delay amplifier of the triggering and
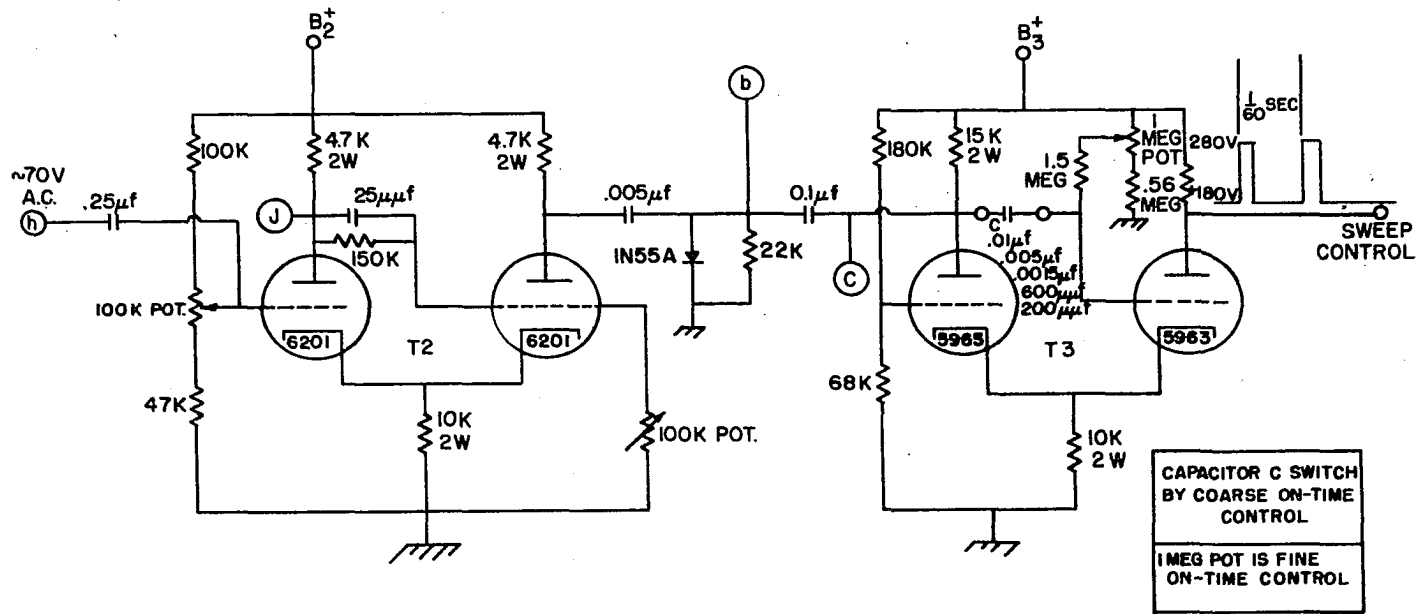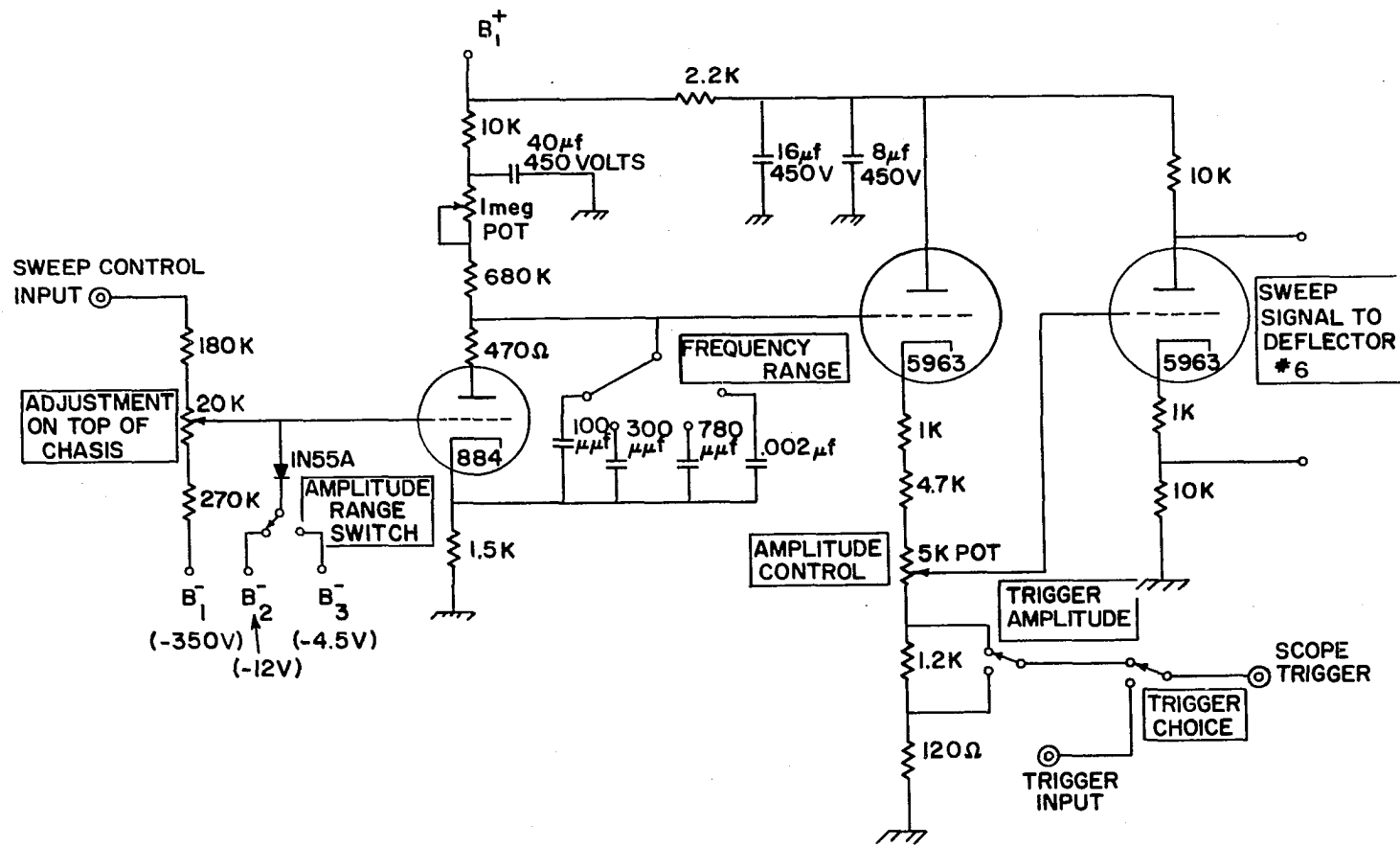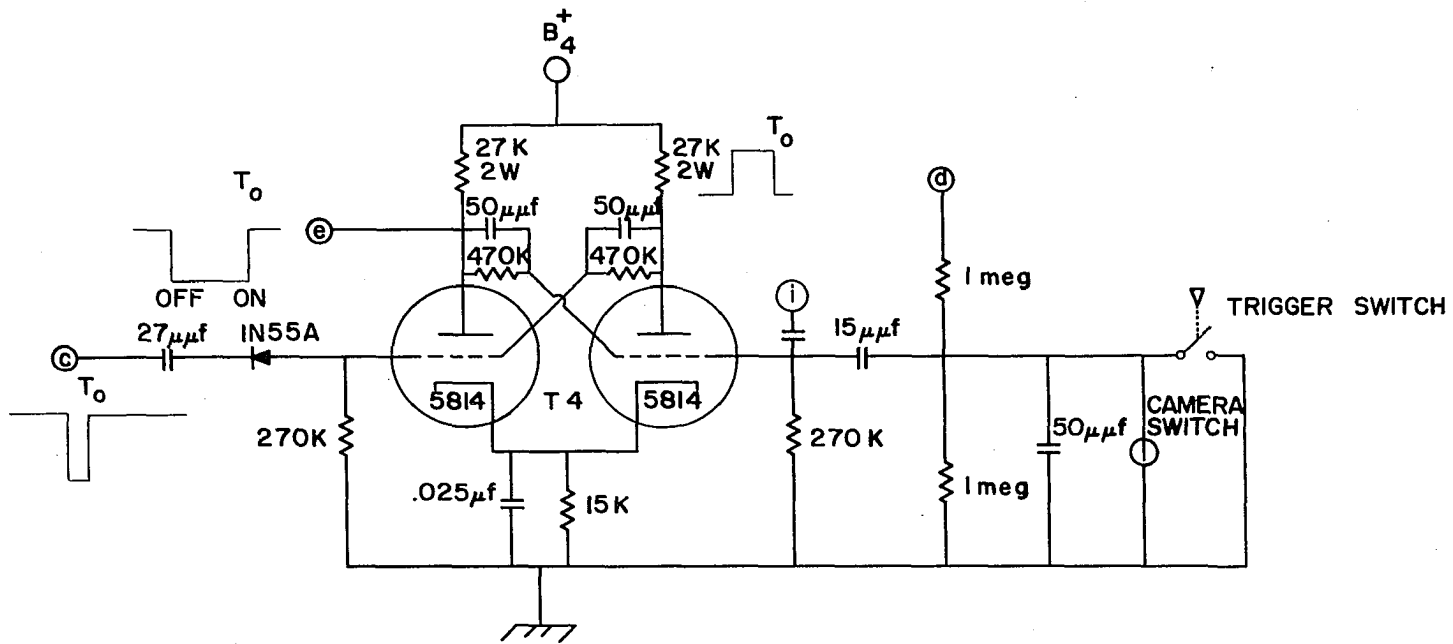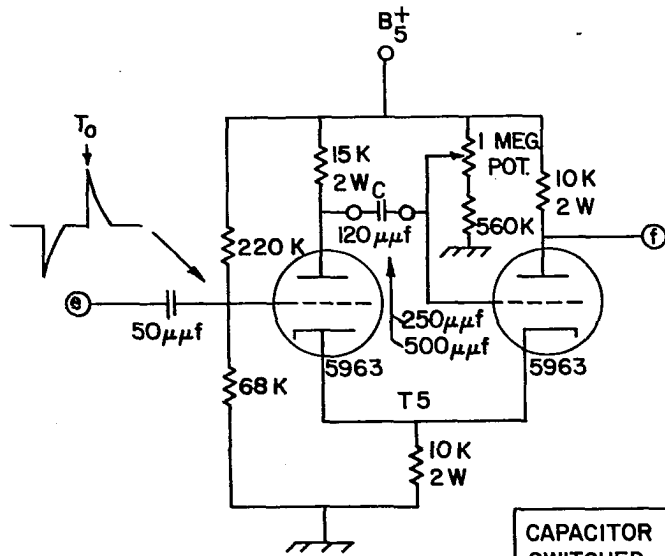   synchronization assembly

CAPACITOR C
SWITCHED BY
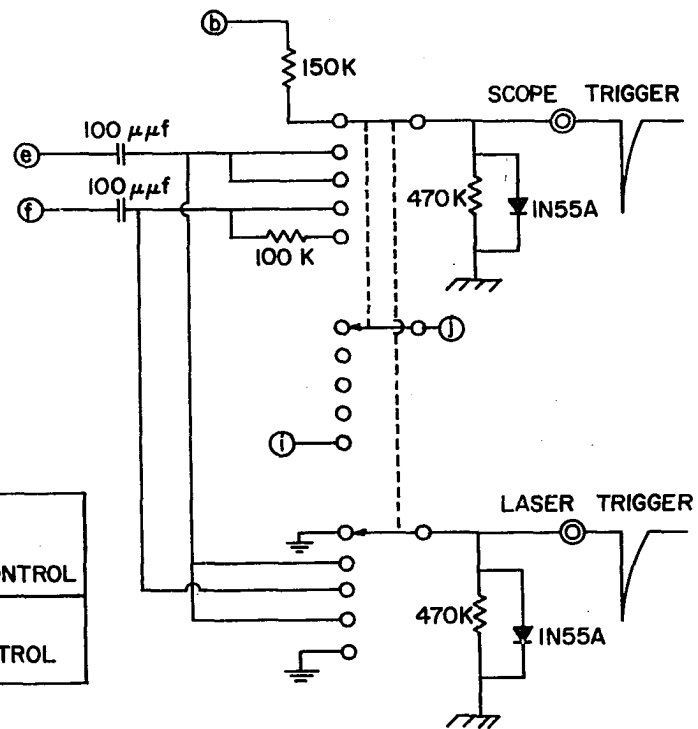COARSE DELAY CONTROL

1 MEG. POT. IS
FINE DELAY CONTROL

72

Figure 22. Circuit diagram of a power supply for the triggering and synchronization assembly

STANCOR
PM
8405

5V RMS

540 V
C. T.

5Y3

6.3 V RMS
C.T.

a

a

320V

750Ω POT
25 WATTS

40μf
450 V

4.7K

40μf
450 V

285 V
0.2 V

O B⁺₁

V. R. TUBE
OA2

V. R. TUBE
OA2

300 V
(RIPPLE-
2V)

d

1K

40μf
450 V

O B⁺₂

285 V
0.2 V

1K

30μf
450 V

O B⁺₃

290 V
0.1 to
0.3 V

4.7K

30μf
450 V

O B⁺₄

275 V

0.02 V

1K

30μf
450 V
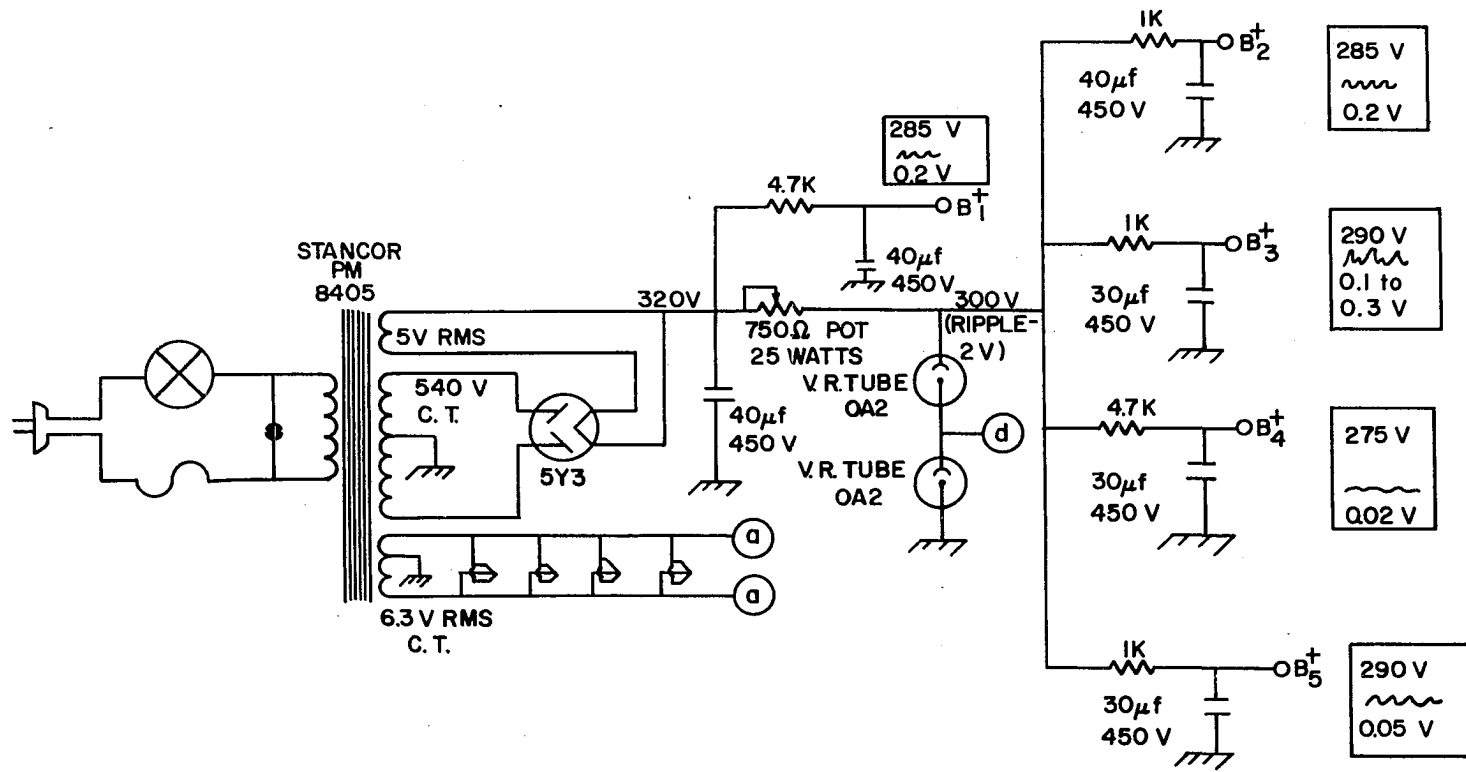
O B⁺₅

290 V
0.05 V

74

Figure 23. Circuit diagram of the power supply for the electron
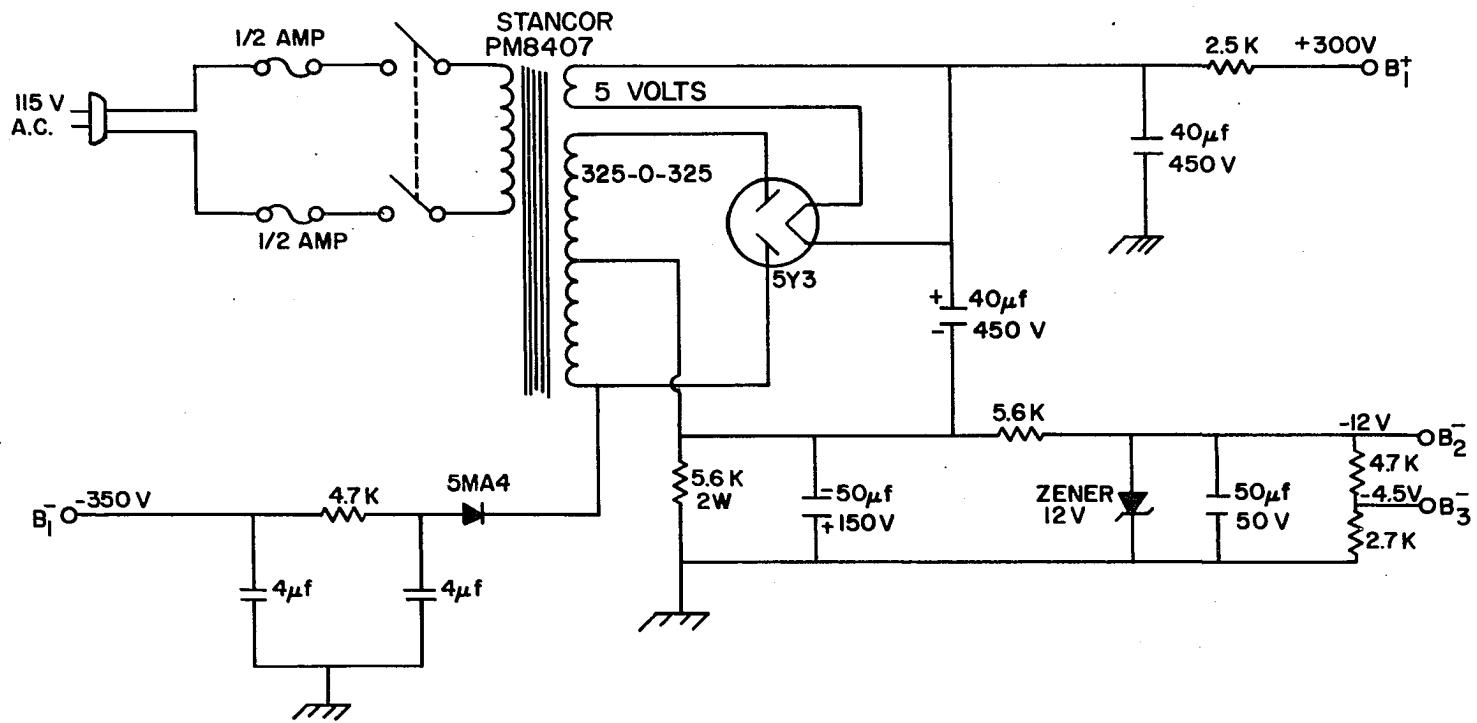beam sweep generator and amplifier

Figure 24. Circuit diagram of the special amplifier to produce
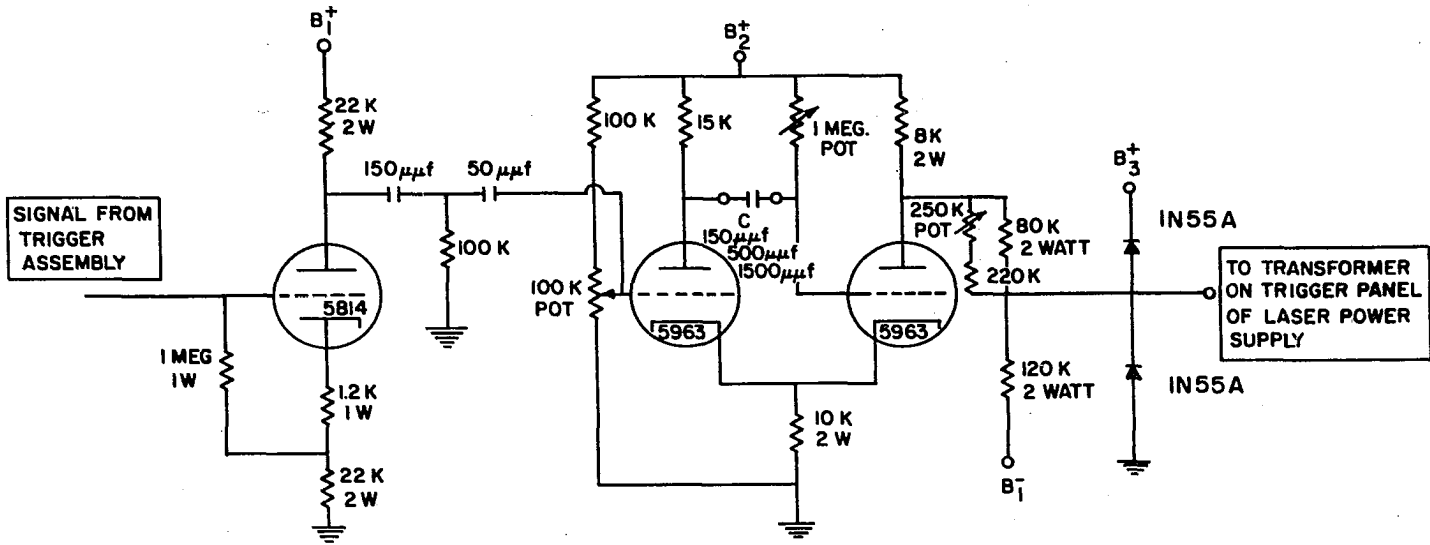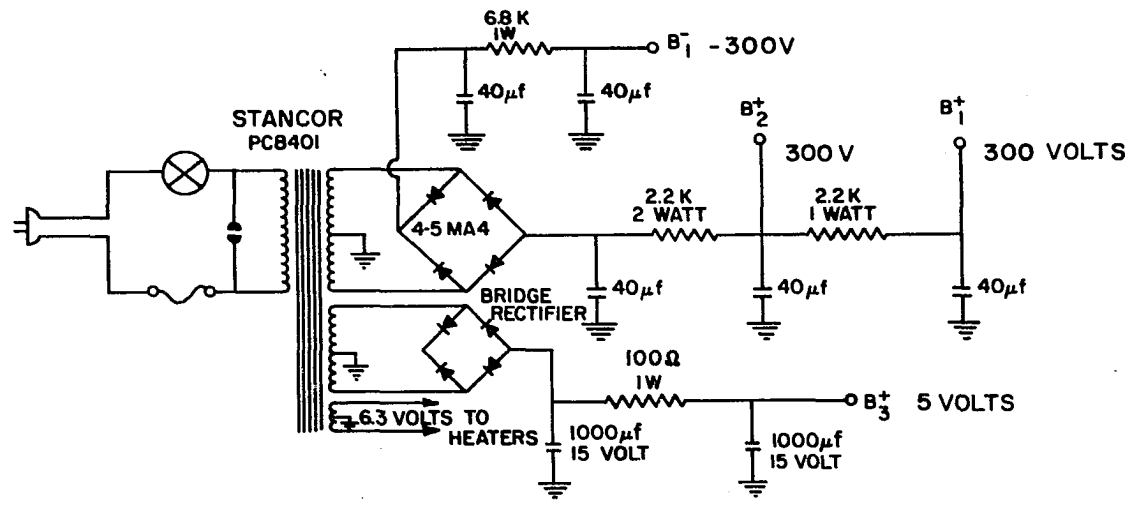a triggering signal for the Korad K-1 laser

Figure 25. Schematic diagram of the pulses used in the
triggering and synchronization assembly

60 CYCLE SIGNAL OF POWER SOURCES	6.3 VOLTS A.C.	
PHASE SHIFT AMPLIFIER	70 VOLTS A.C.	SELECT AND MAINTAIN 60 CYCLE DISTURBANCE
SCHMIDT TRIGGER	+20 VOLTS / −20 VOLTS	PRODUCE WORKING SIGNAL
SWEEP CONTROL GENERATOR	+280 VOLTS / +180 VOLTS	LIMIT PRODUCTION OF SWEEP VOLTAGE
BEAM SWEEP GENERATOR	+20 VOLTS / −20 VOLTS	SAW-TOOTH VOLTAGE FOR ELECTRON DETECTOR
FLIP-FLOP TRIGGER	−20 VOLTS	SYNCHRONIZE SWEEP SCOPE AND LASER
SCOPE TRIGGER	−20 VOLTS	SIGNAL SWEEP OF OSCILLISCOPE
LASER TRIGGER	+20 VOLTS	TRIGGER FLASH-LAMP ON LASER
SCOPE DELAY WITH LASER TRIGGER		FAST SWEEP EXPERIMENTS
SCOPE TRIGGER WITH LASER DELAY		TEST PURPOSES

$\vdash \dfrac{1}{60}$ SECOND $\longrightarrow \dashv$

equilibrium temperature. Finally, a synchronization of laser triggering, oscilloscope triggering and electron beam sweep was required. The laser was triggered at a time so that the giant laser pulse occurred during the electron scan. The signal to start an oscilloscope sweep occurred at the beginning of the electron scan. A final alternative in this circuit complex was a delay mechanism, constructed to allow an oscilloscope triggering pulse to follow a laser triggering pulse or vice-versa. Delayed triggering was rarely used and no further description will be given.

Laser detection systems

An RCA 1P28 photomultiplier was placed behind the passive dye cell assembly to monitor laser radiation. Small laser light losses at the porro prism were intense enough to give a strong photomultiplier signal. Photomultiplier signals, with a load resistor of 5K ohms, were coupled with a 6C4 cathode follower. Pulses were measured with a carefully balanced oscilloscope probe and a Tektronix 551 oscilloscope with a type G plug-in amplifier. When operating the laser in the giant, or Q-switched mode, adjustments were greatly facilitated by the use of a simple integrator with a time constant of about 1000 microseconds. The integrator-detector responded to semi-giant and giant pulses, and the vertical signal was proportional to burst or pulse energy. Each semi-giant pulse appeared as a step function on an oscilloscope trace. Integrated signals were used as a guide to adjust the cryptocyanine dye concentration to obtain single, high energy pulses.

An accurate means of monitoring laser power was by measuring pulse duration and pulse energy. The 551 oscilloscope was, however, inadequate

to measure laser pulse characteristics. For this reason, a second photo-multiplier and oscilloscope were used to measure pulse shapes. An RCA C70042B photomultiplier, operated at 1700 volts, with a load resistor of 75 ohms, was placed behind the electron diffraction porro prism. An impedance matched lead introduced photomultiplier signal into a fast 517A Tektronix oscilloscope. Rise times in the vicinity of 5 to 7 nano-seconds enabled accurate measurement of laser pulse characteristics.

Techniques

Geometry adjustment

It is useful at this time to mention a few characteristics of the laser employed and to present some numerical results from the theoretical treatment of the theory section. The Bragg angle for 1640 volt electrons scattered by standing waves of 6943 Å ruby radiation is 4.35×10^{-5} radians. Hence, the total scattering angle, 2θ, is equal to 8.7×10^{-5} radians. If the electrons encountered perfect Bragg planes the width of the laser cavity, the Bragg condition would impose severe requirements on alignment. For example, if a single mode existed in the laser cavity, the electrons would have to intersect a standing wave plane at the Bragg angle of 4.35×10^{-5} radians for maximum diffraction. If the alignment were off by 1.5×10^{-5} radians, the deflection probability would be de-creased by a factor of two, and the probabilities would fall rapidly to zero at larger misalignment. It would be virtually impossible to attain and preserve such a critical alignment under laboratory conditions. The picture is somewhat more encouraging when the multi-mode nature of our laser is considered. Laser wavelength spreads, according to literature supplied by the Korad company, were perhaps about 0.02 Å. Laser beam

divergences from the laser axis were found for the cavity used in this work to be of the order of 4×10^{-3} radians. The divergent radiation reflected back on itself by the internal prism gives rise to a superposition of Bragg planes with normals distributed over a range of $\pm 4 \times 10^{-3}$ radians to the laser axis. Bragg reflections are then presumably possible over a range of orientations of the electron beam. Although alignment problems are thereby liberalized by the laser divergences, the effective laser power is distributed over many different planes. Consequently, with a multi-mode laser system, much higher powers are required to obtain a given electron reflection probability than with a single mode system. In the divergent system all planes do not, as a rule, possess equal scattering powers. If axial modes are strong compared with off-axial modes, the calculated probabilities for stimulated Compton scattering will be greatest when the electron beam is aligned to be essentially perpendicular to the laser axis.

Two possible adjustments could be made in the present experiment to insure the proper alignment of the electron and laser beams. First, deflector 1 could be used to govern the angle at which electrons traveled through the unit. Second, the entire laser was mounted on a support that could be adjusted to vary the angle at which the laser beam intersected the electron beam. The laser could be tilted as a unit without disturbing its optical alignment. For electron alignment purposes, two collimating platinum apertures, 0.007 inches by 0.25 inches, were mounted two inches apart near the internal porro prism. These apertures were affixed so that electrons passing through both slits would be perpendicular to the laser axis. As the laser angle was changed by moving the support,

the platinum apertures also moved to stay aligned with the laser compo-

nents. Therefore, the beam alignment consisted of arbitrarily setting

deflector 1 and changing laser angle until electron passage through the

two collimating platinum apertures was maximized. In this manner, the

angle between the two beams could be adjusted to be made perpendicular

to within 10^{-3} radians.

Calibration of scattering angle

Stimulated Compton scattering was expected to deflect electrons in

either of two directions, with momentum exchange occurring only along

the axis of the laser cavity. The angle expected between the incident

electron beam and the deflected beam was ϕ_{KD}, 8.7 x 10^{-5} radians. As the

electrons were swept through the detection slit, the incident and deflec-

ted beams would be separated in time as measured by the scintillator,

photomultiplier, and oscilloscope. The time difference would be a function

of the sweep amplitude and the sweep frequency. Because of this, it was

advantageous to calibrate the oscilloscope scale against ϕ, the angle

of scattering, for representative electron sweep adjustments. The

calibration was accomplished by adding a signal to deflector 4, and

measuring the displacement of the focussed beam from lens 4. The elec-

tron beam was observed on a phosphor plate placed on top of lens 6.

When potential differences of tens of volts were applied across deflec-

tor 4, the deflection of the electron beam was of the order of millimeters

and was readily measurable. If linearity were assumed, the voltage re-

quired to deflect the electron beam by the ϕ_{KD} angle could be calculated.

This small voltage could then be applied, and the corresponding displace-

ment on the oscilloscope scale could be determined. With our lens system and typical lens adjustments, the voltage required on deflector 4 to give a scattering angle of ϕ_{KD} was 0.13 volts. As a check, a deflector was temporarily placed at the spot at which the laser radiation and electrons ordinarily intersect. From simple deflector theory, the voltage required to deflect the electrons 8.7×10^{-5} radians was determined. The two calibrations agreed within about ten per cent. The discrepancies arise from uncertainties in the exact position of the principal planes of the thick lens 4 and the edge effect corrections in the laser cavity deflector. Even though electron sweep signals were constant from day to day, the calibration gave variable time differences between the incident and calibrator deflected electron beams. This discrepancy can be attributed to the high magnification introduced by lens 6. A small variation in the adjustable focal plane of lens 4 would cause a relatively great variation in the object distance for the short focal length lens 6. This magnification variation added to the uncertainty of the scattering angle calibration.

Under typical conditions, with oscilloscope sweeps set at 40 microseconds per centimeter, the ϕ_{KD} scattering angle corresponded to a displacement on the oscilloscope trace of 1.6 centimeters. Limits for the calibration were set at ±0.5 centimeters.

Determination of laser characteristics

Although preliminary experiments were done with normal burst laser outputs, the main research was carried out using giant or semi-giant pulses. Only the characteristics of these pulses need be described, the

most important of which are pulse energy, pulse power, beam divergence, and beam area. Pulse energies were monitored by the integrator-detector, a system which had been calibrated with a calorimeter. The calorimeter was an ink-filled polyethylene bag which was shielded from atmospheric convection by styrafoam with a glass window to admit laser radiation. Temperature changes were measured with a thermopile and a K2 potentiometer. The thermopile, which was vibrated at a constant rate, also served to stir the calorimeter fluid. A vertical deflection of 0.23 volts in the integrator-detector corresponded to one joule of energy. The detector was operated under uniform conditions, the calibration was constant, and the laser energy was readily known. A special photomultiplier, which was previously described, gave accurate pulse shapes of the laser bursts. Once the energy and duration of radiation were determined, the calculation of laser power was simple. Divergences of laser output were crudely investigated with the aid of burn spots which occurred when high flux radiation struck a blackened surface such as carbon paper. Black paper was placed on the etalon holder, the window support, and the ruby holders to absorb radiation leaving the laser cavity. An estimate of the laser divergence was determined from the size of the burn spot and the geometry of the laser cavity. Table 3 summarizes laser specifications and laser characteristics.

Table 3. List of laser characteristics for the Korad K-1 laser
operated in the giant pulse mode

.Ruby size	9/16 inch diameter, 4 inches long
Type of ruby	0.05 per cent chromium doped
Wavelength	6943 Å
Wavelength spread[a]	0.02 Å
Primary cavity length	19 inches
Secondary cavity length	approximately 20 inches
Energy of pulse[b]	0.8 - 1.0 joules
Half-height pulse width[c]	10 - 14 nanoseconds
Power of giant pulse[d]	80 megawatts (peak power)
Divergence [e]	4×10^{-3} radians (half angle)
Jitter	20 - 50 microseconds
Q-switching mechanism	passive dye cell
Dye used	cryptocyanine in methanol
Orientation of ruby	"c" axis is horizontal
Polarization	E vector is vertical
Temperature of operation	room temperature

[a] from specifications supplied by manufacturer

[b] determined experimentally with integrator-detector

[c] determined with photomultiplier and fast Tektronix 517A oscilloscope

[d] calculated from pulse energy and half-height pulse width

[e] determined experimentally with aid of "burn spots"

RESULTS

Figure 26 (b) is an oscillogram of the electron beam and laser

beam detector signals recorded with a Tektronix 551 dual beam oscillo-

scope. The lower trace is the signal from the electron detection photo-

multiplier and shows the pulse generated when the electron beam was swept

past the detector slit. Time increases from left to right with one cen-

timeter corresponding to 40 microseconds. The upper trace displays an

integrated signal from the laser energy detector. The integrated signal

serves two purposes; it indicates the energy in a laser pulse and also

indicates the time at which laser action occurred. Since the laser pulse

lasts 10 to 40 nanoseconds and electrons can be deflected only during

laser action, only a minute range of scattering angles can be investi-

gated on any single oscillogram. A large number of separate attempts

are required at various scattering angles to establish the angular de-

pendency of the scattering. Oscillograms (b) and (d) in Figure 26 are

those of attempts to measure electron deflections. The large pulse

corresponding to the undiffracted electron beam serves as a reference

from which the angle of a scattering event can be determined. Figure

24 (c) is a double exposure; one peak shows the position of a normal

incident electron beam, whereas the second peak shows an electron beam

which has been deflected 8.7×10^{-5} radians. This calibration shows that

8.7×10^{-5} radians of electron deflection will appear approximately 1.5

centimeters from the reference or incident electron beam. Oscillograms

(b) and (d) show deflected electrons occurring during laser action.

The electron coincidence in (b) is not immediately evident because

Figure 26. Sample oscillograms from study of stimulated Compton scattering. (a) Response
of photomultiplier with fast 517A Tektronix oscilloscope to show pulse shape
of giant laser pulse. Oscilloscope sweep at 200 nanoseconds per centimeter.
(b) and (d) Upper trace, response of integrator-detector to show energy of giant
laser pulse. Lower trace, contour of electron beam as monitored by scintillation
electron detector. Oscilloscope sweep set at 40 microseconds per centimeter.
Deflected electrons coincident with laser action. (c) Double exposure showing
ϕ_{KD} scattering angle calibration. Oscilloscope sweep set at 40 microseconds per
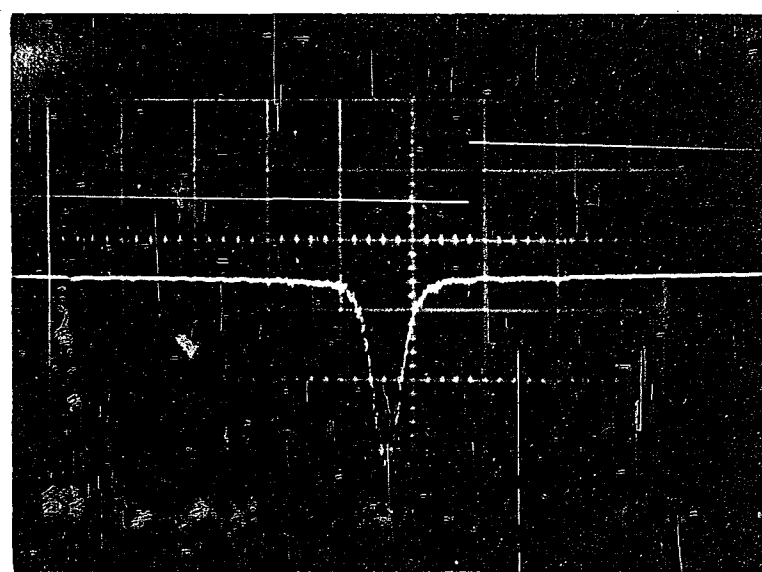centimeter.
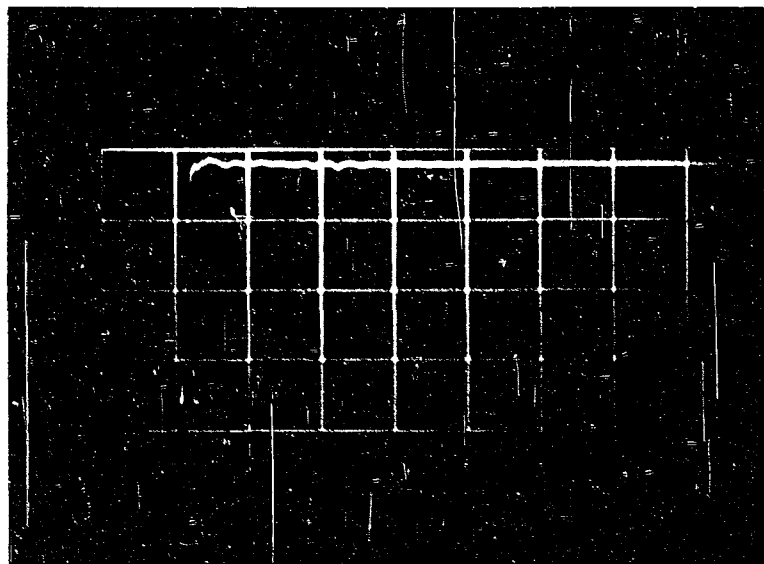
(a)
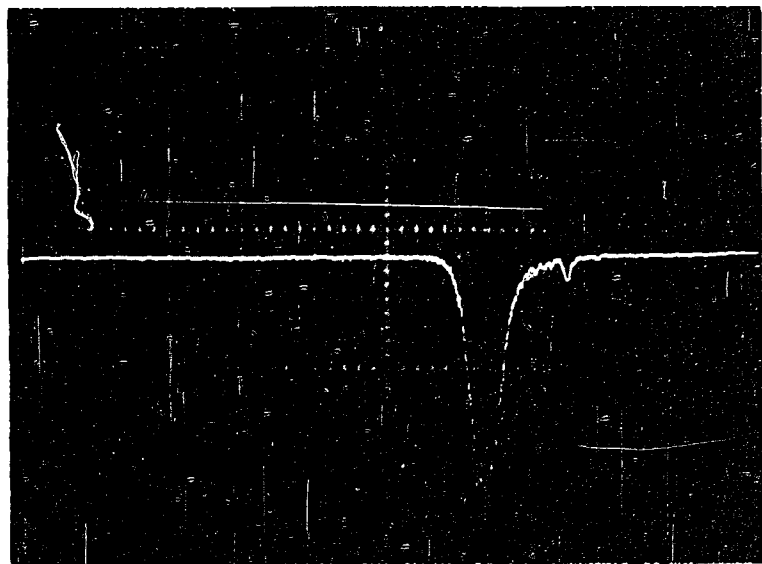
(b)
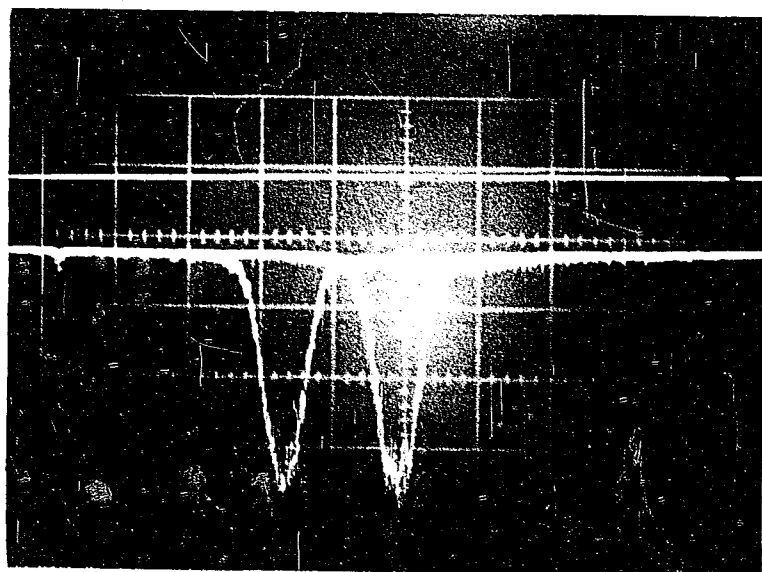
(c)

(d)

some resolution was lost when the picture was reproduced, but neverthe-less, close inspection will indicate a deflected electron peak which is about twelve per cent of the total electron peak. This same slide also illustrates an event which is delayed twelve microseconds after the laser pulse. When the laser pulse is allowed to strike metal portions of the unit, various charged species and gases are removed from the surfaces (9-16). If these particles moved near the electron beam, presumably electron deflections and scatterings cause the electron beam to move over the electron detector slit. These spurious events were diminished by proper alignment to prevent laser radiation from striking the metal surfaces close to the electron beam. When spurious events did occur, they were distinguished because of their delayed occurrence. The spurious results just mentioned, however, led to an earlier misinterpretation of experimental results (17).

Figure 26 (a) gives the oscilloscope response observed when a fast Tektronix 517A oscilloscope in conjunction with a special photomultiplier recorded the shape of a giant laser pulse. In most cases, the pulse was symmetrical and an estimation of laser power was obtained from the laser energy and half-height pulse time.

Many separate experiments were completed over the period of several months when the laser was consistently generating giant laser pulses. Over 200 frames were taken which canvassed both positive and negative scattering angles. Of these, 87 showed electron deflections coincident with laser pulses; 46 indicated that 10 to 25 per cent of the incident electrons were deflected, 38 were events in the 5 to 10 per cent range, and three were recorded with intensities less than five per cent of the

total electron beam.   In order for an event to be counted as a provisional Kapitza-Dirac interaction, the signal had to meet two criteria. First, the event had to occur simultaneously with the laser pulse, and second, the width of the signal had to be a fraction of a microsecond wide. The simultaneity between the laser pulse and the event signal could be measured coincident to within two microseconds. This was unfortunate because the laser pulse lasted only 0.02 microseconds.

In a simple analysis, deflections were plotted as a function of scattering angle and a distribution of scattered electrons was determined. This method was, however, not completely satisfactory because sampling was not constant over all angles. A final analysis took into account the unequal sampling in different ranges of angle. The sum of deflected electron beam intensities for each 0.1 ϕ_{KD} range of scattering angles was divided by the number of observations in the same scattering range. Although the number of separate trials was not sufficient to obtain a smooth and precise distribution function, some meaningful compensation for unequal sampling was possible. Figure 27 presents plots of the observed electron deflections.

The character of the experiment is summarized in the following list of observations.

(a) Deflected electrons were not observed unless very high laser powers were generated. Normal burst peak power outputs of approximately 0.25 megawatts were insufficient to deflect a measurable number of electrons. With 80 megawatts of peak power in a single laser pulse distributed non-uniformly over an area of approximately two square centimeters, often up to 20 per cent of the incident electrons were observed to be

Figure 27. Plot showing deflected electrons which are interpretted as the result
of stimulated Compton scattering. (a) Distribution of angles at which
experimental attempts were made to measure scattered electrons.
(b) A plot of the observed scattering events. Both the scattering angles
and the intensities are indicated. (c) A statistical average intensity
in an attempt to compensate for a non-uniform sampling. The average
intensity in each range of 0.1 ϕ_{KD} is plotted. (note: In the scattering
range of 0.24-0.48 ϕ_{KD}, approximately 25 per cent of the frames were
rendered inconclusive due to high noise events.)

RELATIVE SCALE -- ELECTRON INTENSITY
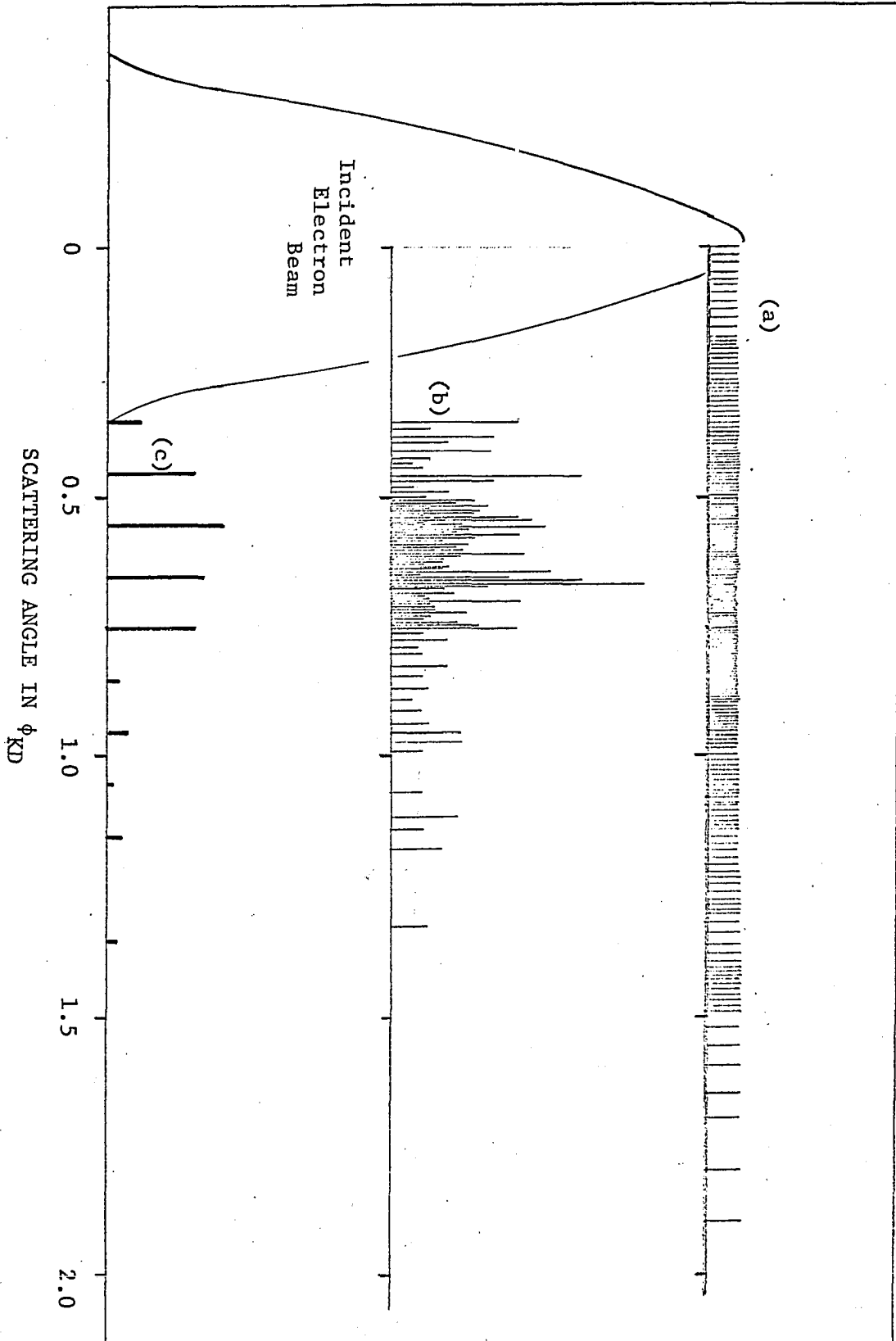
deflected. In approximately 50 attempts, total laser powers were decreased to 15-40 megawatts. Diffracted electrons were observed on nine occasions, but the deflection events were certainly less frequent and lower in intensity than those observed at higher laser powers.

(b) The near perpendicular alignment of the electron beam to the laser axis was essential for the observation of deflected electrons. Unfortunately, the alignment could be trusted to only $\pm 10^{-3}$ radians. Many times when no interactions could be found, a check of alignment revealed a misalignment. After proper alignment was restored, strong deflections could be observed.

(c) Improper laser cable positioning resulted in a magnetic field which presumably changed the angle of electron incidence. In general, strong electron deflections were not observed until the cables were adjusted so that the electron beam suffered only negligible disturbances during laser operation.

(d) Often laser outputs contained a "hot spot". Than is, for some unknown reason, an area of less than 0.5 square centimeters of the total output area contained a much larger radiation density. The energy detector assessed a total energy of the laser output. The "hot spot" contained a higher light intensity at the cost of reducing energy over other portions of the beam. If the "hot spots" were present, electrons were observed to be deflected only if the electron beam passed through the "hot spot".

(e) Precise optical alignment of laser components seemed advantageous, even though total powers were not increased. In one case, a poor window in the second cavity frustrated attempts to observe deflected

electrons, but after the poor window was replaced with a better one, deflected electrons were observed.

(f) Although some frames contained spurious events, perhaps half gave no indication of these events. A majority of frames illustrating deflected electrons was taken only after great care was used in aiming the laser to avoid striking metal portions of the electron diffraction unit.

(g) Although the scintillator and the photomultiplier contributed to electron detection trace noise, the major noise appeared from unfocused or stray electrons inside the electron diffraction unit. With a well focused electron beam, the noise events could be kept to two to five per cent of the total electron trace. It is presumed that most of these noise signals were single electron events, and at most, two electrons contributed to a five per cent noise signal. At large scattering angles, the electron noise events diminished in frequency.

(h) Only a small number of electrons actually intersected the laser beam. Electron beam currents were measured near the electron detector with a Faraday cage. It was estimated that approximately 40 electrons which entered the laser cavity during the ten nanoseconds of intense laser radiation, actually made it through the detection slit. Therefore, a deflection probability of 0.2 for stimulated Compton scattering allows only about eight electrons to be deflected.

DISCUSSION

It may be advantageous to describe a hypothetical plot similar to
Figure 27 which would present very strong evidence that observed deflec-
ted electrons were truly the result of stimulated Compton scattering.
An incident electron beam would have a small divergence as compared with
ϕ_{KD}. The envelope of deflected electrons would appear at an angle of
8.7×10^{-5} radians from the incident beam with a general absence of
electrons between the two peaks. A less than ideal set of conditions
could also present good evidence for the documentation of stimulated Com-
ton scattering. If an electron beam existed with an angular spread of
8.7×10^{-5} radians, an envelope of deflected electrons would just be re-
solved from the main beam. Although no gap would exist between the in-
cident and diffracted peaks to confirm a general absence of electron
events, the fact that the diffracted envelope resembled the main or in-
cident beam and was centered on the expected scattering angle would
constitute fair evidence that stimulated Compton scattering was being
observed.

In this study, laboratory conditions were not ideal, but somewhat
similar to the less than ideal set of conditions just described.
Figure 27 shows that the average electron beam spread was slightly less
than 10^{-4} radians. A distribution of deflected electron events peaks
at an angle smaller than the expected ϕ_{KD} angle. The scattering angle
calibration, however, may well have an uncertainty of the order of 40
per cent. Therefore, the observed deflections are not grossly incon-
sistent with the expected angle of deflection. The shape of the proba-

bility distribution for the observed deflections is also useful in diagnosing the nature of the observed signals. The distribution should resemble the undeflected beam except for the broadening effects of experimental instabilities in the diffraction angle calibration factor. There is little doubt that the observed peak decreases in intensity at angles larger than ϕ_{KD}. The possibility of irregularities at angles small than ϕ_{KD} must, however, be explored. Some question arises about the possibility of observing deflected electrons if the angle of deflection is comparable with the breadth of the incident beam. Small signals of four per cent can be observed in the electron trace except where the slope of the incident electron trace is changing. It is estimated that at the most unfavorable slope of the electron beam trace, an eight per cent signal could be obscured. On the basis of experimental data, the distribution of deflected electrons approaches zero at scattering angles of less than ϕ_{KD}. The plot in Figure 27 is in accordance with expectations and does constitute fair evidence that stimulated Compton scattering was truly being observed.

A small number of electron deflection events appear at a relatively large scattering angle. It is plausible that an electron can undergo two first order deflections and be deflected by the angle $2\phi_{KD}$. Since a whole distribution of standing light waves is present, a deflected electron can intersect a second standing wave at the Bragg angle and undergo a second deflection. One would expect that the dual deflections would be more difficult to obtain and much less frequent than single electron scattering events. The resolution, however, of the experiment was poor and one could not expect to resolve the first and pseudo second order reflections.

With a wavelength spread of 0.02 Å, 80 megawatts of laser power
uniformly spread over about 1.4 square centimeter of area, and a diver-
gence of four milliradians; the theoretical probability of electron
deflection is equal to approximately 0.07. It is not unreasonable, how-
ever, that up to 20 per cent of the incident electrons could be deflec-
ted. One needs only to consider the inhomogeneities of the laser output.
The "hot spots" are the clearest demonstration that certain portions of
the laser output contain higher intensities and lower divergences than
the assumed uniform distributions of both intensity and divergence in
the above calculation. Increased laser intensities coupled with lower
divergences could easily give calculated electron deflection probabil-
ities of 20 per cent. In experiments, strong events were observed
when the electron beam intersected "hot spots", whereas events did not
exceed the noise level when the electron beam intersected the weaker
portions of the laser output. Laser outputs, even though free of "hot
spots" were presumed to be non-uniform. It is believed that axial and
near-axial modes are appreciably higher in power than off-axial modes.
Therefore, the strongest interactions were likely to occur when the elec-
tron beam was aligned to intersect Bragg planes composed of the stronger,
less divergent radiation. If these less divergent components of the
laser beam accounted for the observable electron scatterings, the lati-
tude in electron alignment would be more critical than the latitude cal-
culated from the divergence of the overall laser output.

All the experimental observations are apparently consistent with
developed theory. A critical test of theoretical expressions, however,
was not possible because the complex distribution of energy and

divergence of the laser radiation were not adequately characterized. Carefully controlled experiments were hampered by the uncertainty in electron alignment and the inhomogeneities and irregularities of the laser radiation. Hopefully, laser technology will perfect a laser with greater uniformity and reproducibility in divergence and power so that better documentation of stimulated Compton scattering can be possible.

SUMMARY

The phenomenon of stimulated Compton scattering of electrons, i.e. the diffraction of electrons by standing light waves, was predicted by Kapitza and Dirac 30 years ago. Until the advent of the laser as an intense and coherent light source, the experimental observation of stimulated Compton scattering remained hopelessly beyond the scope of experimental reality. The intense standing waves set up inside a laser cavity, however, would seem well suited for an experimental test of the proposal of Kapitza and Dirac.

Kapitza and Dirac derived a probability for interaction by coupling the known probability for ordinary Compton scattering with the ratio of Einstein coefficients for stimulated and spontaneous emission. This formulation of Kapitza and Dirac was not directly applicable to representative experimental conditions in which a laser is used as a light source. Stimulated Compton scattering has since been treated in this laboratory in terms of an interaction of an electron plane wave with a perturbing potential corresponding to the standing light wave to obtain a stationary state solution to the Schroedinger equation. Probabilities of electron deflection were derived for various laboratory conditions with emphasis placed on electron beam orientation and coherence properties of the laser.

A new electron diffraction unit has been designed for the observation of stimulated Compton scattering. Giant pulses in the cavity of a Q-switched ruby laser served to diffract 1640 volt electrons. The small scattering angles were measured by scanning the electrons past a slit of

a scintillator detector. Theoretical demands on design of apparatus are discussed, experimental difficulties are listed, and the limitations of the apparatus are described.

Numerous experiments were completed over the period of several months when the laser generated high powers. Many deflection events were obtained at both positive and negative scattering angles which were consistent with expectations for stimulated Compton scattering. Some experiments were attempted in which the electron deflection probabilities were observed as functions of electron beam orientation and laser power. Qualitative results indicated that measurable electron deflections occurred only when the electron beam intersected intense standing light wave planes at the Bragg angle. The observed deflections also required high laser powers. All experimental observations seemed consistent with developed theory within the broad limits of experimental error. A critical test of theoretical expressions, however, was not possible because the complex distribution of energy and divergence of the laser radiation were not fully characterized.

Although good evidence has been gathered to verify the existence of stimulated Compton scattering, the investigation is not complete. More experiments are likely to follow elsewhere with improved lasers. The experience gained in this investigation should be instrumental in designing a much improved apparatus.

BIBLIOGRAPHY

1. Kapitza, P. L. and Dirac, P. A. M., Proceedings Cambridge Philosophical Society 29, 297 (1933).

2. Compton, A. H., Physical Reviews 21, 207, 483, 715 (1923).

3. Compton, A. H., Physical Reviews 22, 409 (1923).

4. Compton, A. H., National Academy of Sciences; Proceedings 10, 271 (1924).

5. Born, M., Zhurnal Physik 38, 803 (1926).

6. Everhart, T. E. and Thornley, R. F. M., Journal of Scientific Instruments 37, 246 (1960).

7. Kafalas, P., Masters, J. I., and Murray, E. M. E., Journal of Applied Physics 35, 2349 (1964).

8. Soffer, B. H., Journal of Applied Physics 35, 2551 (1964).

9. Chang, T. Y. and Birdsall, C. K., Applied Physics Letters 5, 171 (1964).

10. Ready, J. F., Industrial Research 7, 44 (1965).

11. Honig, R. E., Applied Physics Letters 3, 8 (1963).

12. Ready, J. F., Applied Physics Letters 3, 11 (1963).

13. Giori, F., MacKenzie, L. A., and KcKinney, E. J., Applied Physics Letters 3, 25 (1963).

14. Lindor, William L., Applied Physics Letters 3, 210 (1963).

15. Lichtman, D. and Ready, J. F., Applied Physics Letters 3, 115 (1963).

16. Verber, C. M. and Adelman, A. H., Journal of Applied Physics 36, 1522 (1965).

17. Bartell, L. S., Thompson, H. B., and Roskos, R. R., Physical Review Letters 14, 851 (1965).

ACKNOWLEDGEMENTS

I wish to express my sincere appreciation to Dr. L. S. Bartell for suggesting this study and for his valuable advice and assistance throughout my studies.

I want to recognize the help of Dr. H. Bradford Thompson in designing the original model of the electron diffraction unit and the electronic circuits, and in helping with a large number of the preliminary experiments. I would also like to acknowledge the assistance of Miss Jean Jacob in assembling some of the circuits.

I am indebted to the many fellow graduate students and friends who shared both my trials and triumphs during the past several years.

I sincerely thank my parents for their generous help and their constant encouragement.

Finally, I wish to thank my fiancee, Miss Betty Dworschak, to whom I dedicate this work, for the concern and understanding she has shown and the cheerful support she has given throughout this study.